

High–Velocity Clouds: Building Blocks of the Local Group

Leo Blitz¹

University of California, Berkeley, CA 94720
University of Maryland, College Park, MD 20742

David N. Spergel²

Princeton University Observatory, Princeton, NJ 08544
University of Maryland, College Park, MD 20742

Peter J. Teuben³

University of Maryland, College Park, MD 20742

Dap Hartmann⁴

Harvard-Smithsonian Center for Astrophysics, Cambridge, MA 02138

W. Butler Burton⁵

Leiden University Observatory, Leiden, Netherlands

Received _____; accepted _____

ABSTRACT

We suggest that the high–velocity clouds (HVCs) are large clouds, with typical diameters of 25 kpc and containing 5×10^7 solar masses of neutral gas and 3×10^8 solar masses of dark matter, falling onto the Local Group; altogether the HVCs contain 10^{11} solar masses of neutral gas. Our reexamination of the Local–Group hypothesis for the HVCs connects their properties to the hierarchical structure formation scenario and to the gas seen in absorption towards quasars.

We begin by showing that at least one HVC complex (besides the Magellanic Stream) must be extragalactic at a distance >40 kpc from the Galactic center,

¹blitz@gmc.berkeley.edu

²dns@astro.princeton.edu

³teuben@astro.umd.edu

⁴dap@abitibi.harvard.edu

⁵burton@strw.leidenuniv.nl

with a diameter >20 kpc and a mass $>10^8$ solar masses. We then discuss a number of other clouds that are positionally associated with the Local Group galaxies. The kinematics of the entire ensemble of HVCs is inconsistent with a Galactic origin, but implies that the HVCs are falling towards the Local Group barycenter. The HVCs obey an angular–size/velocity relation consistent with the Local Group infall model.

We simulate the dynamical evolution of the Local Group. The simulated properties of material falling into the Local Group reproduce the location of two of the three most significant groupings of clouds and the kinematics of the entire cloud ensemble (excluding the Magellanic Stream). We interpret the third grouping (the A, C, and M complexes) as tidally unstable nearby material falling onto the Galactic disk. We interpret the more distant HVCs as dark matter “mini–halos” moving along filaments towards the Local Group. Most poor galaxy groups should contain HI structures to large distances bound to the group. We suggest that the HVCs are local analogues of the Lyman–limit absorbing clouds observed against distant quasars.

We argue that there is a Galactic fountain in the Milky Way, but that the fountain does not explain the origin of the HVCs. Our analysis of the HI data leads to the detection of a vertical infall of low–velocity gas towards the plane. We suggest that the fountain is a local phenomenon involving neutral gas with characteristic velocities of 6 km s^{-1} rather than 100 km s^{-1} . This implies that the chemical evolution of the Galactic disk is governed by episodic infall of metal-poor HVC gas that only slowly mixes with the rest of the interstellar medium.

The Local–Group infall hypothesis makes a number of testable predictions. The HVCs should have sub-solar metallicities. Their $\text{H}\alpha$ emission should be less than that seen from the Magellanic Stream. The clouds should not be seen in absorption to nearby stars. The clouds should be detectable in both emission and absorption around other groups. We show that current observations are consistent with these predictions and discuss future tests.

Subject headings: Galaxy: general, formation, evolution, and structure — Local Group — intergalactic medium — ISM: clouds, high–velocity clouds, structure, kinematics and dynamics — quasars: absorption lines

1. Introduction

Since their discovery in 1963 by Muller, Oort, & Raimond, the nature of the high-velocity hydrogen clouds (HVCs) has remained a mystery. HVCs are clouds that deviate from Galactic circular rotation by as much as several hundred kilometers per second. Although astronomers have speculated about the origin of HVCs since their detection, no single explanation has encompassed the vast quantity of data that has been collected on the clouds (see Wakker & van Woerden 1997, hereafter WvW97, and references therein). Particularly important is the lack of agreement on a characteristic distance for the clouds, because most of the relevant physical parameters depend on distance to one order or another. In the 1970s, a well-defined subset of the clouds was identified as a tidal stream associated with the Magellanic Clouds (Mathewson, Cleary, & Murray 1974), but since then no consensus has arisen regarding the nature of the remaining clouds which constitute the majority of HVCs.

In this paper, we suggest that the HVCs represent infall of the intergalactic medium onto the Local Group. Previous authors have explored the possibility that the HVCs are infalling primordial gas (Oort 1966, 1970) and have associated the HVCs with the Local Group (Verschuur 1969; Kerr & Sullivan 1969; Arp 1985; Bajaja, Morras, & Pöppel 1987; Arp & Sulentic 1991), but subsequent observations always produced fundamental difficulties for the particular models considered. Here, we assemble evidence based on new general-purpose surveys of atomic hydrogen gas by Stark et al. (1992) and by Hartmann & Burton (1997), and on the HVC surveys by Hulsbosch & Wakker (1988) and by Bajaja et al. (1985), and consider theoretical arguments in the context of modern cosmology. We argue that the clouds are matter accreting onto the Local Group of galaxies. Their velocities would thus largely reflect the motion of the clouds in the gravitational potential of the Local Group and the motion of the LSR about the Galactic center. We suggest that the clouds represent the building blocks from which the Local Group was assembled and that they continue to fuel star formation in the disk of the Milky Way.

The evidence is presented as follows. In Section 2, we review some of the observed properties of the high-velocity clouds, and indicate those which are not consistent with a Galactic origin for the HVCs. In Section 3, we detail the observations entering our analysis. In Section 4, we discuss the stability of the HVCs against gravitational collapse and against Galactic tidal forces, and suggest that these considerations imply that the most of the clouds are extragalactic at distances typical of the Local Group. The stability criteria imply, however, that the largest clouds are nearby and possibly are interacting with the Milky Way. In Section 5, we discuss three individual clouds, one of which must be beyond the disk of the Milky Way, and two others that appear to be associated with M31 and M33,

suggesting that at least some of the HVCs may be extragalactic. We identify a subset of the HVCs centered near the barycenter of the Local Group, and show that its kinematics as well as that of the entire HVC ensemble are well described as being at rest with respect to the Local–Group Standard of Rest (LGSR); the kinematics are thus inconsistent with a Galactic origin. The entire HVC ensemble is also shown to exhibit an angular–size/velocity relation consistent with membership in the Local Group. In Section 6, we simulate the accretion history of the Local Group and show that the simulation accounts for the observed distribution and kinematics of the HVC ensemble. The agreement between the simulation and the observations supports inferences about similarities between the Local Group HVCs and the Ly- α absorbing clouds observed toward quasars. We show that the velocity extrema observed for the HVCs are consistent with their membership in the Local Group. In Section 7, we discuss the distances and abundances of the HVCs in the context of the Local Group HVC hypothesis, and show that the hypothesis is consistent with all of the observations made to date. We review extragalactic HI searches for HVCs which have revealed clouds with properties similar to those we derive, in about the expected numbers. In Section 8, we discuss the implied mass accretion rate, and implications for the chemical evolution of the disk of the the Milky Way. We also present evidence for the Galactic fountain in low–velocity HI which suggests that the HI disk of the Milky Way is not in hydrostatic equilibrium. In Section 9, we conclude by discussing predictions and future tests of the model, and summarize the principal arguments made in this paper.

2. High–Velocity–Cloud Properties

HVCs are HI clouds with radial velocities inconsistent with circular or near–circular rotation about the Galactic center, and in this and other regards unlike most of the HI making up the Galactic disk. Perhaps the most useful kinematic definition is that of the “deviation velocity” introduced by Wakker (1991), indicating the degree to which a cloud deviates from a reasonable circular–rotation model. We note the following general properties of HVCs other than those which are part of the Magellanic Stream (see WvW97 for a thorough review):

- (1) HVCs have LSR radial velocities as extreme as -464 km s^{-1} . The most extreme radial velocity consistent with circular rotation is about $\pm 220 \text{ km s}^{-1}$.
- (2) HVCs have both positive and negative radial velocities, but clouds with positive radial velocities are distributed differently on the sky than clouds with negative velocities.
- (3) Two HVC complexes (The Magellanic Stream and Complex C) are contiguous

structures covering thousands of square degrees on the sky. Most HVCs, however, have angular extents of a few square degrees or less. Individual clouds separated by several or tens of degrees are often separated in velocity by hundreds of kilometers per second. Except for the Magellanic Stream, the largest cloud complexes tend to lie at positive latitudes in the first and second Galactic quadrants; these include the well known complexes A, C, and M, which have received the most observational attention. We refer to these clouds as the Northern Hemisphere Clouds and find them to be the nearest examples of the HVC phenomenon (see §4.2.

(4) HVCs have a narrow range of internal velocity dispersions, centered near 13 km s^{-1} (see Section 4).

(5) HVCs have low dust-to-gas ratios, at least a factor of three below that of normal Galactic clouds (Wakker & Boulanger 1986).

(6) Measured heavy-element abundances are all well below solar values. Although few metallicities are available, those measured are also significantly subsolar.

(7) Distance measurements to the clouds have been largely indeterminate, although several recent observations in the direction of Northern Hemisphere Clouds suggest a distance of about 5 kpc for Complex A (van Woerden et al. 1998) as well as for Complex M (Danly, Albert, & Kuntz 1993).

Clearly, any explanation of the nature and origin of the HVCs must account for these observed properties. Previous explanations fall into two broad categories: Galactic and extragalactic. In the first general discussion of the nature of the HVCs, Oort (1966) realized that if the clouds are self-gravitating then they must have distances on the order of a Mpc. In Galactic models, of which the most popular is the Galactic fountain (Shapiro & Field 1976; Bregman 1980), the HVCs would be too near to be bound by their own gravity and, because of their large internal velocity dispersions, would be transient objects with typical lifetimes $\lesssim 10^6 \text{ y}$. It is difficult to understand in the Galactic fountain context why the clouds would not be metal rich or how their vertical velocities would be greater than 70 to 100 km s^{-1} . Extragalactic models, on the other hand, generally require HVCs to be gravitationally stable for periods comparable to a Hubble time, and to be metal poor (though not necessarily with zero metallicity).

3. HI Observations

Our analysis relies principally on the catalogue of HVCs compiled by Wakker & van Woerden (1991, hereafter WvW91) and on the new Leiden/Dwingeloo survey of HI of Hartmann & Burton (1997, hereafter LD). The WvW91 compilation is based largely on data from the HI survey of Hulsbosch & Wakker (1988), made with the Dwingeloo 25-m telescope over the northern sky at 1° intervals covering LSR velocities from -900 to $+800$ km s^{-1} with a velocity resolution of 8.25 km s^{-1} , together with data from the HI survey of Bajaja et al. (1985), made with the Villa Elisa 100-foot telescope over declinations only accessible from the southern hemisphere, at somewhat coarser resolution and somewhat lower sensitivity. The Wakker & van Woerden catalogue also includes data from a number of other observational programs covering specific HVCs in enhanced detail.

The Leiden/Dwingeloo HI survey of Hartmann & Burton (1997) utilized the Dwingeloo 25-m telescope to observe the sky at declinations north of -30° , at the relatively high resolutions of 0.5 in angle and 1 km s^{-1} in velocity, covering the velocity range $-450 < v_{\text{LSR}} < +400$ km s^{-1} . Although the velocity coverage of the LD survey is less than that of WvW91, few HVCs have been found beyond the negative-velocity range of the LD survey, and none beyond the positive-velocity edge. The sidelobe response has been removed from the LD data by subtracting, from each spectrum, the simulated sidelobe response of a modeled telescope antenna to a full-sky HI map (Hartmann 1994; Hartmann et al. 1996). Although the survey was motivated by problems pertaining to the Milky Way, it is useful for some HVC studies too. When smoothed to the resolution of the Hulsbosch & Wakker data, the sensitivity of the LD data is similar; its superior spatial and velocity resolution makes it particularly useful for obtaining observational parameters of some of the HVCs. The LD survey has not, however, been analyzed for high-velocity emission in the detail of WvW91.

We also utilize the Bell Telephone Laboratories HI survey of Stark et al. (1992, hereafter BTL), which was the first northern hemisphere HI sky survey with full beamwidth sampling and low sidelobe response. Although the rather coarse (2°) angular resolution is not particularly well-suited to investigations of most HVCs, the velocity resolution of 5 km s^{-1} is not a disadvantage in global HVC studies because most HVC lines are considerably broader than this. The BTL and LD surveys have similar noise levels when convolved to the same resolution. Although possible sidelobe contamination is not particularly worrisome for HI features with velocities beyond those of conventional Galactic emission, low sidelobe response is useful for studying those HVCs seen at high Galactic latitudes within the velocity range of Galactic plane HI. We checked the reality of weak features by making cross comparisons between the BTL and LD surveys.

4. Stability Criteria for the HVCs

We begin our analysis by calculating the characteristic self-gravitating distances for the HVCs. As mentioned above, Oort (1966) noted that self-gravitating HVCs imply that the HVCs are at a distance of \geq Mpc. Giovanelli (1979), using better HI data, argued that the virial distances would place many HVCs outside the Local Group. Here, we revisit the calculation with new data and include the presence of dark matter in our analysis.

If the HVCs are objects nearly as old as the Universe, they must be gravitationally and tidally stable for a Hubble time. A self-gravitating cloud obeys the relationship

$$v_{3D}^2 < \frac{2GM_{\text{HI}}}{fR} \quad (1)$$

where M_{HI} is the mass in neutral hydrogen, f is the hydrogen/total mass ratio, and R is the gravitational radius of the cloud. Because HVCs are not sites of star formation nor has CO ever been found associated with them (Wakker et al. 1997), the inequality in equation (1) is reversed for HVCs. The equation can therefore be used to estimate an upper limit to the distance of an HVC, assuming that it is self-gravitating:

$$r_g < 88.6 \frac{f\Delta v}{T_B\Omega^{1/2}} \text{ kpc}, \quad (2)$$

where Δv is the observed FWHM of the HI emission from a cloud, measured in km s^{-1} , T_B is the peak HI brightness temperature, measured in K, and Ω is the solid angle projected by the cloud in square degrees; the coefficient includes a 40% correction by mass for helium.

Stable clouds must also be able to withstand the shear of the Galactic tidal field; this consideration yields a lower limit to the distance of an HVC:

$$-\frac{d}{dr}\left(\frac{\Theta^2}{r}\right)R < \frac{GM}{R^2}. \quad (3)$$

This implies, in terms of observables:

$$r_t > 24.8 \frac{\Theta^2\Omega^{1/2}f}{T_B\Delta v} \text{ pc}, \quad (4)$$

where r is the distance to the cloud and Θ is the circular speed of the Galaxy at the distance of an HVC. If one assumes that $\Theta = \Theta_\odot$ for $r_t < r_c$, where r_c is the distance where the rotation curve becomes Keplerian, and that $\Theta^2 = r_c\Theta_\odot^2/r_t$ for $r_t > r_c$, then for $r_c = 100$ kpc, equation (4) becomes

$$r_t > 1.34 \times 10^3 \frac{\Omega^{1/4} \Theta_{\odot} f^{1/2}}{(T_B \Delta v)^{1/2}} \text{ pc}, \quad (5)$$

for $r > 100$ kpc, and where equation (4) holds for $r < 100$ kpc. For $r_t < r_g$, only the gravitational distance is important, because clouds that are not gravitationally stable are also not tidally stable.

If f is sufficiently small that either dark matter or ionized gas dominates the mass of an individual HVC, that is, if the mass of the cloud is given by Rv_{3D}^2/G independent of its distance, then the tidal criterion becomes a criterion on the angular size of an HVC:

$$\Omega < 7.13 \times 10^3 \frac{\Delta v}{\Theta_{\odot}^2} \text{ sq deg}, \quad (6)$$

for $R < 100$ kpc, and

$$\Omega < 7.13 \times 10^3 \frac{\Delta v}{\Theta_{\odot}^2} \frac{R}{100 \text{ kpc}} \text{ sq deg}, \quad (7)$$

for $R > 100$ kpc, assuming a rotation curve flat to 100 kpc.

An additional useful relation is the crossing time, t_c , for the cloud, defined as the timescale for which a cloud would double in size if it were not self gravitating:

$$t_c = 17.1 \frac{\Omega^{1/2} r_{\text{kpc}}}{\Delta v} \text{ My}, \quad (8)$$

where r_{kpc} is the distance to the cloud in kpc.

4.1. HVC Statistics

We first consider the statistics of the clouds to determine mean observational quantities, T_B , Ω , and Δv . We use the WvW91 compilation because of the better spatial resolution compared to the BTL catalogue. However, the line width is not explicitly given and must be estimated from the total flux and T_{max} . Histograms of these quantities are given in Figure 1. The statistical properties are given in Table 1. We have checked the distribution of these quantities with the BTL compilation and find good agreement between the two catalogues given their differences between them.

From Figure 1, as well as from Table 1, it is clear that the mean and median of both T_B and Ω are quite different, which is reflected in the dispersion of these quantities. The

means are dominated by the skewed distribution and a few very large values. We obtain representative values of the observed quantities from the means of $\log T_B$, $\log \Omega$ and $\log \Delta v$, which give values close to the medians of the observed quantities. Note the narrowness of the distribution of velocity dispersion; this small dispersion occurs in both the BTL and WvW91 data and suggests that the HVCs as a whole are a single collection of objects with similar intrinsic properties.

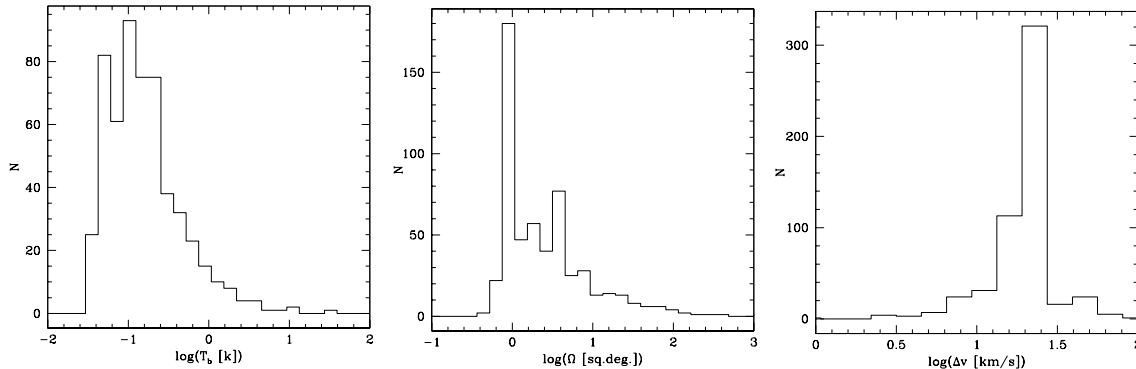


Fig. 1.— *Left:* Histogram of brightness temperature (in K) for the HVCs in the WvW91 compilation. *Center:* Histogram of solid angle (in square degrees) subtended by the HVCs in the WvW91 compilation. *Right:* Distribution of average linewidths (FWHM) (in km s^{-1}) for the HVCs in the WvW91 compilation.

We now wish to determine the mean values of r_g and r_t . In the WvW91 compilation we eliminate the clouds for which we do not have a good estimate of Δv : clouds with $\Omega > 100$ sq deg (where which the assumption that T_{max} is a representative temperature over most of the cloud probably breaks down). This introduces only a small bias because there are only nine clouds with such large areas. Histograms of the results are shown in Figure 2. In the BTL sample, we eliminate unresolved clouds, which leaves 444 clouds from the sample of 1312. As a check we also calculate r_g , and r_t from the mean of the log cloud properties in Table 1. A summary of the results is given in Table 2. All three methods give consistent determinations of these quantities.

We note first that $r_t < r_g$ for the great majority of clouds; thus the tidal distance is generally unimportant. The typical value of r_g is of the order of $6f$ Mpc. If $f = 1$ and the clouds were self-gravitating at this distance, they would, on average, be part of the Hubble flow, they would not exhibit the velocity cutoff described in §5.2.3, and they would also not exhibit the overwhelmingly negative observed velocities relative to the LGSR. A mean distance of $6f$ Mpc is also an order of magnitude larger than the distance to M31 for values of f near unity, and much larger than the 1.5 Mpc radius at which the clouds are turned around from the Hubble flow in the simulations (see Figure 12). However, if the HVCs are

TABLE 1
Mean Observed HVC properties

Quantity	mean	dispersion	median
T_B (K)	0.35	± 0.88	0.14
Ω (sq deg)	16.1	± 133.9	1.9
Δv (km s^{-1})	20.6	± 9.2	20.9

Mean of log HVC properties

T_B (K)	0.16	± 0.28	0.14
Ω (sq deg)	2.5	± 6.8	1.9
Δv (km s^{-1})	18.9	± 10.5	20.9

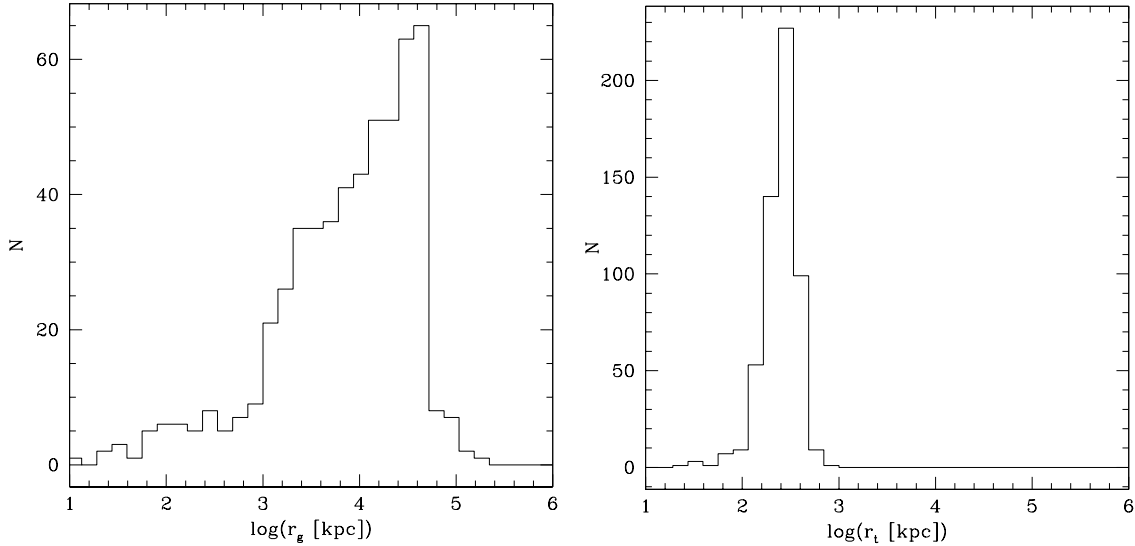


Fig. 2.— *Left*: Histogram of the distribution of distances in kpc at which the neutral hydrogen in an HVC in the WvW91 compilation would make the cloud self gravitating. *Right*: Distribution of distances (in kpc) of the clouds in the WvW91 compilation within which the clouds would have to be if they are tidally stable.

TABLE 2
Stability distances

Quantity	mean	dispersion	median
Wakker–Hulsbosch sample			
r_g (kpc)	$6.5 \times 10^3 f$	± 6.92	$10.0 \times 10^3 f$
r_t (kpc)	$2.5 \times 10^2 f^{1/2}$	± 1.51	$2.7 \times 10^2 f^{1/2}$
BTL sample			
r_g (kpc)	$4.9 \times 10^3 f$	± 3.5	$5.9 \times 10^3 f$
r_t (kpc)	$3.0 \times 10^2 f^{1/2}$	± 2.0	$3.0 \times 10^2 f^{1/2}$
From mean cloud properties			
r_g (kpc)	$6.7 \times 10^3 f$		
r_t (kpc)	$2.1 \times 10^2 f^{1/2}$		

TABLE 3
Mean derived HVC parameters

Quantity	value
Mass	$3.2 \times 10^8 M_\odot$
HI mass	$3.4 \times 10^7 M_\odot$
Diameter	28 kpc
Distance	1 Mpc
$\langle n_{\text{HI}} \rangle$	$1.2 \times 10^{-4} \text{ cm}^{-3}$
f	0.15

extragalactic, we expect that they contain copious amounts of dark matter. Observations of galaxies and clusters suggest that the baryon/dark matter ratio is roughly 0.1 (Fukugita, Hogan, & Peebles 1997). If HVCs are fair samples of material from which galaxies are made, then we expect that $f \sim 0.1$. This implies that their true distance is $\sim 0.5 - 1.0$ Mpc.

Using the mean cloud values, at a typical distance of 1 Mpc the typical diameter of an HVC is about 28 kpc, a large value, but comparable to the value we obtain for Complex H in §5.1.1. At a distance of 1 Mpc, the HVCs have a typical neutral hydrogen mass of $\sim 3.4 \times 10^7 M_\odot$, a value close to the HI mass of Complex H, a total neutral gas mass of $\sim 4.7 \times 10^7 M_\odot$, and a total mass of $\sim 3.2 \times 10^8 M_\odot$. The mean HI density (n_{HI}) of a typical cloud is then $1.2 \times 10^{-4} \text{ cm}^{-3}$. A mean density this small might require some clumpiness for the cloud to remain neutral even in the metagalactic radiation field (see § 7.1.2). The typical derived HVC properties are summarized in Table 3.

4.2. Stability of the Largest HVCs

Although for most HVCs the tidal–stability distance is less than the self–gravitating distance, the opposite is the case for the largest HVCs. Furthermore, for these largest HVCs, the conditions imposed by equations (6) and (7) are so severe that all clouds with angular sizes greater than about 100 sq deg cannot be tidally stable at any reasonable distance. Equation (7) can be rewritten, for example, as

$$0.34 \Omega \Delta v_{20} < \frac{R}{100 \text{ kpc}} \quad (9)$$

where Δv_{20} is the linewidth measured in units of 20 km s^{-1} ; Figure 1 shows that this quantity is generally of order unity. Thus any cloud with an angular size > 60 sq deg will be tidally unstable for any distance < 2 Mpc. Complexes A, C, and M, the three main structures comprising the Northern Hemisphere grouping, are all larger than this: Complex C, for example, covers 1814 sq deg. All three of these complexes in the Northern Hemisphere grouping therefore are tidally unstable for any reasonable distance if they are self–gravitating. The gravitational–binding distance, r_g , is moreover quite small for the largest clouds. For Complex A, which has a mean Δv of $\sim 40 \text{ km s}^{-1}$, and a mean T_B of 1.0 K, $r_g < 85f$ kpc. That is, this cloud cannot be more than 85 kpc distant even if it is self–gravitating by its gas content alone ($f = 1$); if it contains substantial amounts of ionized gas or dark matter, it is probably substantially closer than 85 kpc. For values of f in the range 0.1 to 0.2, Complex A would have a maximum distance of ~ 10 to 15 kpc. If Complexes C and M, together with A, are all part of a single general grouping, then this distance would be consistent with the two measured absorption–line distances to the HVCs by Danly et al. (1993) and by van

Woerden et al. (1997). This distance is also consistent with the large total angular extent of this structure, nearly 180° . If the mean diameter typical of HVCs is about 28 kpc, and if this structure is a typical HVC, then its distance would be < 15 kpc, since it subtends more than 2 radians. We conclude then that the Northern Hemisphere Complex probably has a mean distance of ~ 10 to 15 kpc, an extent of ~ 25 kpc, is being tidally sheared, and traverses a range of distances from the Sun, including some which are evidently as near as several kpc.

These considerations suggest that the HVC Complexes A, C, and M, which have been the most studied of the HVCs because of their large angular extent and location at declinations accessible from northern hemisphere telescopes, are atypical because they are so close; moreover they appear to be interacting with the Milky Way. The proximity to these clouds might also explain why distance determinations to the Northern Hemisphere grouping have been so discrepant, with most absorption–line measurements giving only upper limits: the material is probably strung out over a large range of distances because of its intrinsic size and the tidal shearing.

There are two other complexes with angular sizes in excess of 1000 sq deg: the Outer Arm Complex and the Magellanic Stream. The tidal and gravitational binding considerations discussed above apply equally well to these complexes if they are self–gravitating. In the case of the Outer Arm, it is not clear whether it is really a collection of HVCs, or part of the normal structure and dynamics of the outermost Milky Way. In any event, it must be tidally unstable if it is self–gravitating, and both it and the Magellanic Stream have self–gravitating distances < 100 kpc, possibly considerably less than this. It might even be that the Magellanic Stream is not gas tidally disrupted from either the Milky Way or the LMC, but rather an HVC that has become entrained in the tidal field of the LMC/Milky Way system.

For clouds with angular sizes between ~ 100 and 1000 sq deg, the gravitational binding distance is greater than that for the three largest clouds complexes, and such clouds would be expected to be more distant than Complex A. Complex H, which we discuss in detail in §5.1 has $\Omega = 250$ sq deg, $r_g = 580 f$ kpc, and $r_t = 190 f^{1/2}$ kpc. If Complex H is typical of other HVCs, and f is about 0.1, then $r_g \simeq r_t = 60$ kpc, and its distance would be close to the value of 50 kpc value determined from kinematic considerations in §5.1.1. It seems, therefore, that the stability argument yields some information about distances, and that this information is consistent both with direct distance measurements, in the case of the nearby Northern Hemisphere clouds, with inferences from the kinematics in the case of Complex H, and with cloud properties statistically inferred from numerical simulations.

5. Evidence for Extragalactic Nature of HVCs

5.1. Individual HI features

We consider here three individual clouds seen in the second quadrant of Galactic longitude which suggest that at least some of the HVCs must be extragalactic.

5.1.1. HVC Complex H

Longitude–velocity plots of HI lying near the Galactic equator show that most of the gas in the Milky Way is in nearly–circular orbits about the Galactic center. Figure 3 shows such a plot for LD–survey data over the longitude range $0^\circ \leq l \leq 250^\circ$, averaged over $|b| \leq 10^\circ$. Negative velocities in the longitude range $l = 0^\circ - 180^\circ$ correspond to gas at distances greater than R_\odot , under the assumption of circular rotation; near–circular orbits are suggested by the approximately sinusoidal contours of the HI, especially at the lower contour levels. The most distant gas would contribute the lowest contours, at velocities near $170 \sin l \text{ km s}^{-1}$, corresponding to a distance of about 37 kpc from the Galactic center, if $\Theta(R \geq R_\odot) = \Theta_\odot = 220 \text{ km s}^{-1}$ (or to a distance of about 27 kpc if the rotation curve were to become Keplerian at the last measured point about 20 kpc from the center). Gas with rotation velocities in excess of Θ_\odot cannot be in circular rotation anywhere in the Milky Way. For $\Theta_\odot < 220 \text{ km s}^{-1}$, kinematic distances are increased.

Figure 3 also shows emission, however, from an HI structure, in the longitude range $l = 110^\circ$ to 135° , extending to velocities as high as -240 km s^{-1} , well beyond the most extreme circular–rotation speeds permitted. A map of this HVC material is shown in Figure 4, which integrates all of the HI emission beyond the range of normal circular velocities, from $-240 < v_{\text{LSR}} < -170 \text{ km s}^{-1}$. This structure was first detailed by Hulsbosch (1975) and therefore named Complex H by WvW91. Complex H is quite large, with an angular extent of $\simeq 25^\circ$. (The complex has a somewhat larger extent in the compilation of WvW91 than that shown in Figure 4 because WvW include velocities that are still part of the outermost gas in the Galactic disk.) The radial–velocity centroid of the brightest part of the emission is -200 km s^{-1} ; if this characterizes the systemic velocity of Complex H, and if the higher velocities are due to the velocity dispersion of the HI, the distance from the Galactic center would be about 85 kpc for a flat rotation curve (43 kpc assuming that the rotation curve becomes Keplerian at $R = 20 \text{ kpc}$). In any event, Complex H is quite large, with an angular extent of about 25° and a radial velocity that places it beyond $\sim 50 \text{ kpc}$ from the center, under any reasonable Galactic rotation curve.

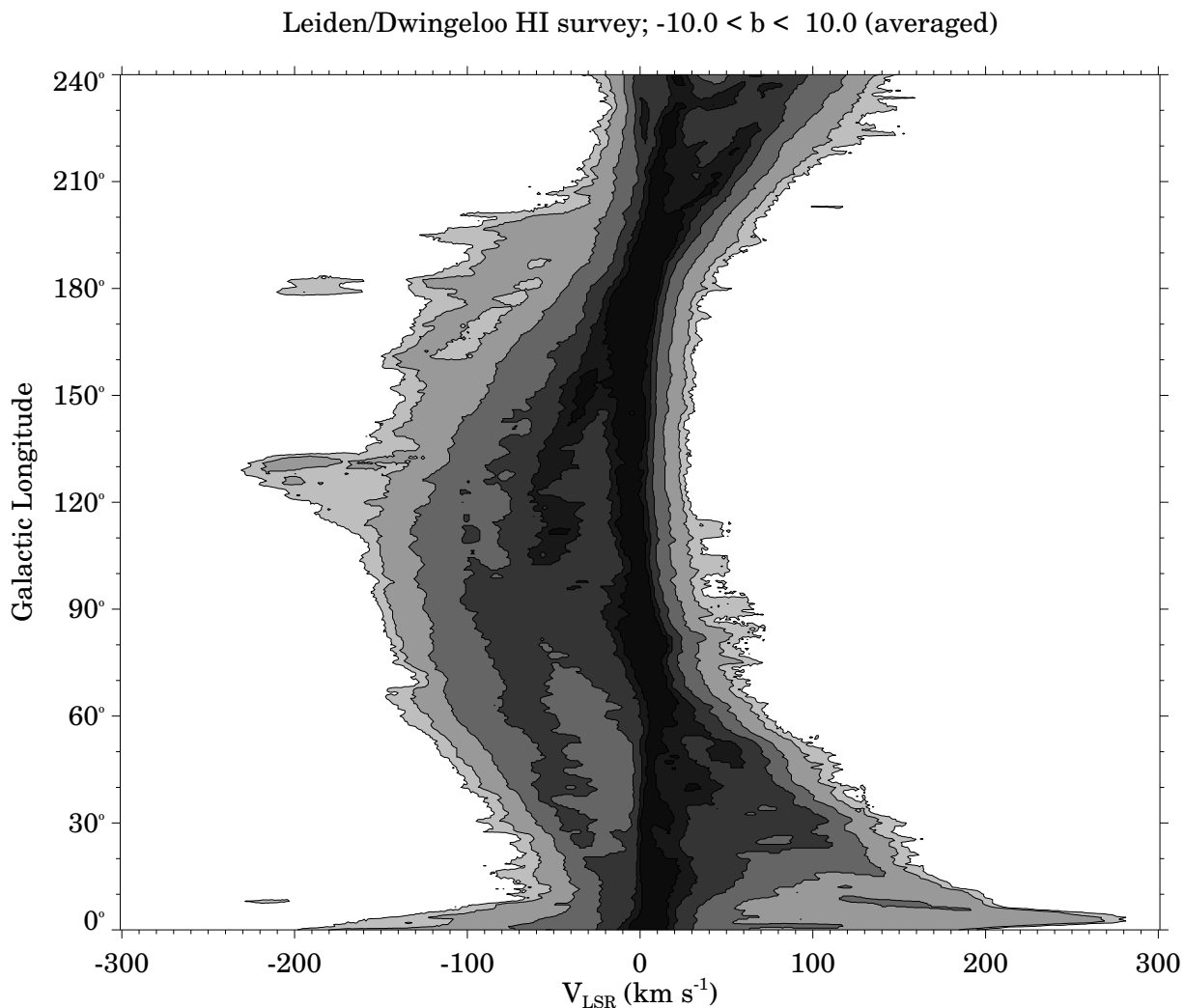


Fig. 3.— Longitude–velocity plot of HI emission from the LD survey averaged in latitude over $|b| \leq 10^\circ$. The contour intervals are spaced logarithmically. Gas at negative velocities for $l < 180^\circ$ corresponds to gas beyond the Sun’s radius in a circular–rotation model. The lowest negative–velocity contours are approximately sinusoidal, indicating nearly circular rotation to a distance of about $R = 40$ kpc for a flat rotation curve. Note, however the emission at $110^\circ < l < 133^\circ$, with velocities up to about -230 km s^{-1} . This is Complex H; higher–sensitivity maps show that the velocity of Complex H extends to -240 km s^{-1} .

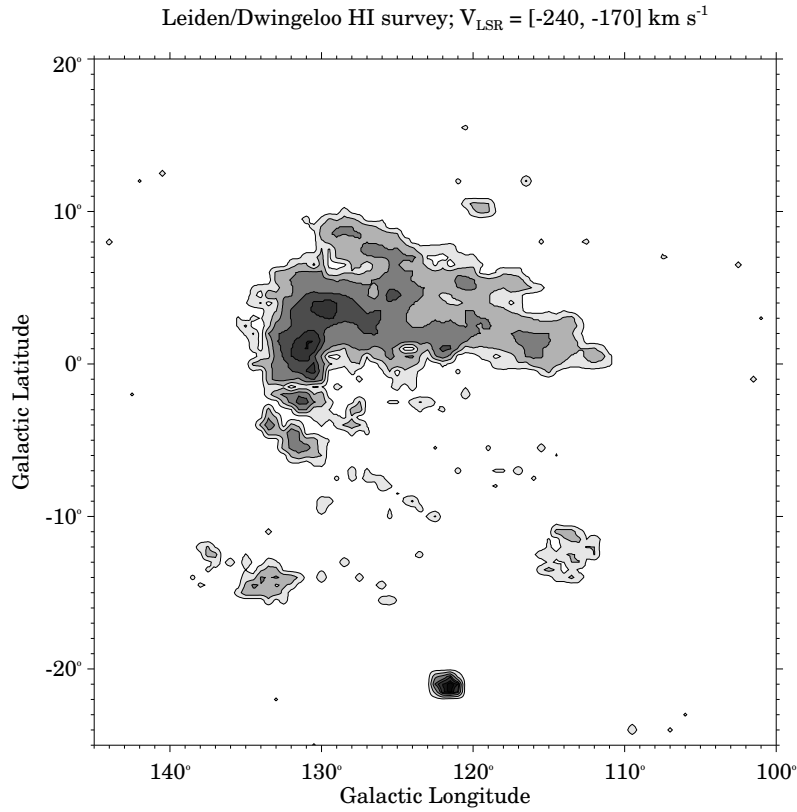


Fig. 4.— HI emission from Complex H integrated over the velocity range $-240 \leq v_{\text{LSR}} \leq -170 \text{ km s}^{-1}$. This range was chosen to exclude the conventional Galactic gaseous disk; parts of Complex H may in fact extend to more extreme velocities. The contour intervals are spaced linearly. The bright object at $l = 122^\circ$, $b = -21^\circ$ represents the portion of M31 emitting within the chosen velocity range.

Because Complex H lies directly in the plane, it is at a minimum distance of 40 kpc from the Galactic center, whether or not its radial velocity corresponds to circular motion. If the complex were at distances smaller than 40 kpc (that is, if the velocity of the cloud has a substantial non-circular component), then the velocity difference between the complex and the ambient Galactic disk gas would range from 30 to 200 km s^{-1} , producing a huge region of highly shocked gas. No major disturbance in the HI images of this part of the disk is apparent, however. One would also expect strong radio-continuum and X-ray emission, and other indicators of strong shocks, but no such shock tracer is evident over the region. $\text{H}\alpha$ or other optical emission would be expected at least at the higher latitudes where the extinction is relatively low, because the high velocity of Complex H relative to the ambient gas would be comparable to that of the jets from young stars, which are all strong optical emitters (Lada 1985). There is no indication that the emission from the disk is anomalous, supporting the conclusion that the complex lies beyond the gaseous disk of the Milky Way.

The large angular size of Complex H implies that, if it is at a distance of 50 kpc from the Sun, then it has a diameter of about 20 kpc and an HI mass of about $9 \times 10^7 M_{\odot}$, using the total HI flux seen in Figure 4, an enormous gas structure by Galactic standards; the mass would scale with the square of the distance. Using equation (2) of §4, the distance of the cloud would be $1.0 f$ Mpc if it were self-gravitating, where f is the ratio of neutral gas/total mass of the structure. Thus f would have to be ~ 0.1 if Complex H were self-gravitating, a value similar to that deduced in §4.1 for the ensemble of HVCs.

5.1.2. Kinematic Distances to Other HVCs

The argument supporting a large distance for Complex H is more difficult to apply to HVCs located out of the Galactic plane. The constraint that Complex H lies beyond the outer edge of the gaseous disk is not applicable to most HVCs because they are largely identified out of the Galactic plane. For example, another HVC with a substantial deviation velocity is seen in Figure 3 near $l = 180^{\circ}$, $v = -180 \text{ km s}^{-1}$; this is the ACI knot in the Anticenter Complex, most of which extends beyond the borders of Figure 3. The ACI concentration is centered only about 10° below the Galactic plane and, as Complex H, shows no association with any disturbance in the conventional gaseous disk. However, because it does not lie directly in the Galactic plane, the constraint on the distance to the ACI knot is weaker than for Complex H.

There have been several suggestions of evidence for interactions of HVC material with the conventional gaseous disk in some of the Northern-Hemisphere Clouds which were argued in §4.2 to be relatively local, but none for the HVCs which we argue are dispersed throughout

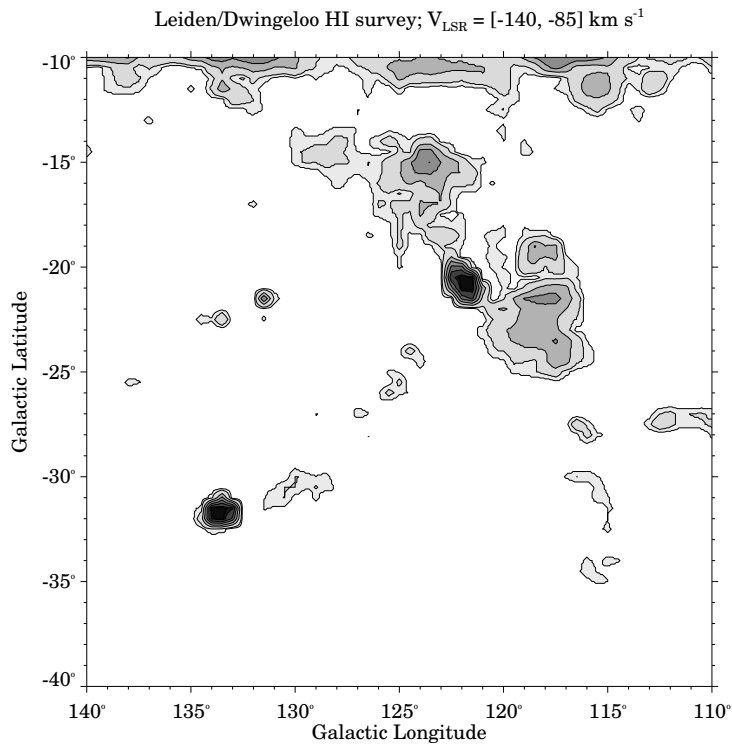
the Local Group (§5.2.2). Burton (1997) discussed two general observational constraints on the distances of high- and intermediate-velocity clouds. The “scale-height constraint” recognizes the measured half-thickness of the HI gaseous disk, which is well-established by the observations to be about 120 pc; if HVCs were a general property of the disk-halo transition region, they would have to be confined to $|z| \leq 100$ pc to be consistent with the measured thickness; otherwise, HVCs would have to occur beyond the disk-halo interface, typically at large enough distances that their existence does not contaminate the scale-height measurement.

5.1.3. HVCs in the Direction of M31

The bright emission feature evident in Figure 4 at $l = 122^\circ, b = -21^\circ$ represents HI in the disk of M31. Could it be that Complex H is part of a tidal tail extending toward Andromeda? We used the BTL and LD surveys to map the HI emission in the general region around M31, but found no HVC feature continuous or nearly continuous in position and velocity comparable to the Magellanic Stream. We did, however, find the remarkable HI halo seen in Figure 5 as it appears in the LD survey, approximately centered on M31, which we discuss below as the M31 Cloud. In this figure, M31 itself is the bright spot in the central region of the cloud, some 2° in extent; M33 is the bright feature at $l = 133^\circ 5, b = -32^\circ$. The gaseous disk of the Milky Way contributes the emission along the top edge of the figure. The M31 Cloud is also seen in the BTL survey and a small portion of it occurs in the WvW91 catalogue.

The extent of the emission surrounding the direction to M31 is about 14° . If the M31 cloud were at the distance of M31, its diameter would be about 170 kpc and its mass about $9 \times 10^8 M_\odot$. The velocity extent of the cloud is $-145 < v_{\text{LSR}} < -80 \text{ km s}^{-1}$; it is therefore not centered on the systemic velocity of M31 ($v_{\text{LSR}} = -300 \text{ km s}^{-1}$), but emission from the cloud does blend with the lower-absolute-velocity side of M31. The apparent blending may, however, be fortuitous: there is no direct evidence for an interaction between the HI cloud and M31, nor is there direct evidence that the cloud and M31 are at the same distance. Because the M31 Cloud does not connect smoothly with Complex H, either spatially or kinematically, it appears likely that the M31 Cloud and Complex H are unrelated.

The positional coincidence of the M31 Cloud with M31 is striking, however, as is the blending in velocity. Not only is the M31 Cloud nearly centered on M31 itself, its position angle on the sky as well as its inclination (if the cloud is disk-like) are both similar to those of M31. These morphological similarities make it reasonable to ask if the cloud is somehow associated with the galaxy. It seems unlikely that the M31 cloud is part of a very extended



hvc_m31_m33_narrow_low 3-OCT-1997 14:50 dap hartmann

Fig. 5.— HI emission in the vicinity of M31 integrated over the velocity range $-140 \leq v_{\text{LSR}} \leq -85 \text{ km s}^{-1}$. HI emission from M31 in this velocity range yields the bright knot of emission at $l = 122^\circ$, $b = -21^\circ$. The extended halo of emission around M31 is the M31 Cloud. The bright knot at $l = 133.5^\circ$, $b = -31.5^\circ$, is the HI emission from M33 in the velocity range plotted. Other smaller HVCs are also evident in the figure; several of them give the appearance of a broken chain extending between M31 and M33. The band of emission across the top of the image represents HI in the gaseous disk of the Milky Way.

gaseous disk of M31, because the cloud has a less extreme systemic velocity than the galaxy proper, and extends well beyond the minor axis on one side of the galaxy, which would not be the case if it were in normal galactic rotation. Furthermore, there is no evidence for the cloud in maps made in the velocities between -300 and -400 km s^{-1} , corresponding to velocities from the approaching, southeast part of the M31 disk. Although the M31 Cloud is superimposed on M31 on the sky, there is no clear evidence for an *interaction* with the galaxy. Nevertheless the location and morphology of the M31 Cloud remain striking.

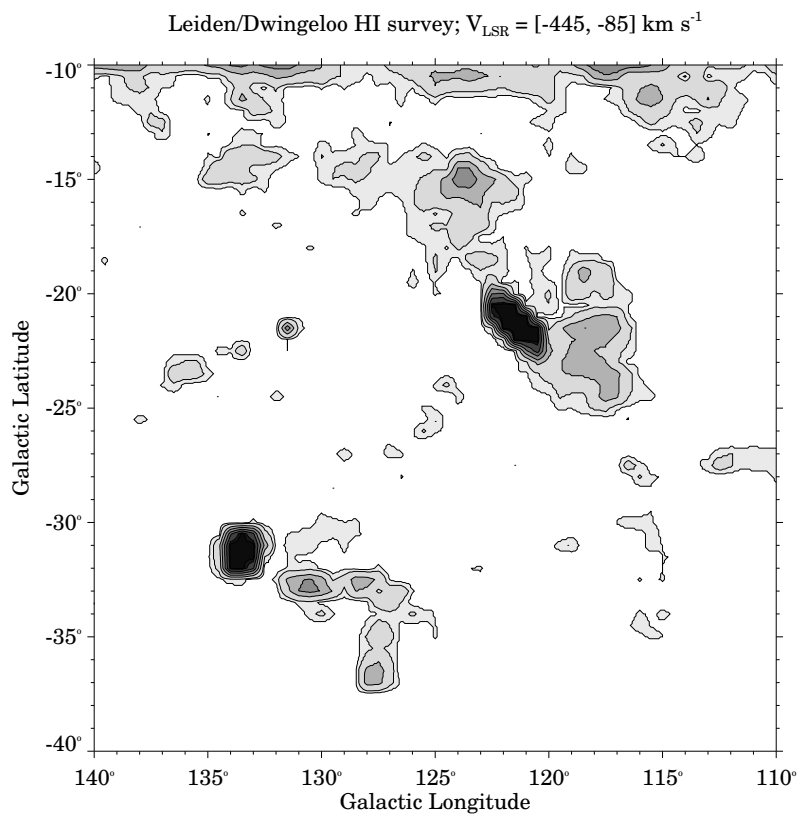
Davies (1975) found a compact HVC in close positional proximity to M31 which he argued is likely to be associated with that galaxy, despite its different velocity. The Davies cloud, with an angular extent of only $0^{\circ}.5$, is within about $1^{\circ}.5$ of the center of M31, but has an LSR velocity of -447 km s^{-1} , as close to the systemic velocity of the galaxy as the M31 Cloud. At the distance of M31, the Davies cloud would have a mass of $4.7 \times 10^6 M_{\odot}$ and a diameter of 5 kpc.

5.1.4. HVCs in the Direction of M33

Close to M33, Wright (1974, 1979) found an HVC in the velocity range $-440 < v_{\text{LSR}} < -320$ km s^{-1} ; the cloud is shown in Figure 6 as it appears in the LD survey. M33 itself is the bright object at $l = 133^{\circ}$, $b = -31^{\circ}.5$; Wright’s cloud is the extended hook-shaped object to the right of, and slightly below, that galaxy. The detailed maps which Wright made of this cloud did not allow him to ascertain whether there is, or is not, any connection between M33 and this very-high-velocity cloud of HI. At the distance of M33 the cloud would have an HI mass of $1.6 \times 10^8 M_{\odot}$ and a diameter of 70 kpc.

Figure 6 also shows several other HVC patches that appear as a broken chain of emission along the line between M31 and M33, suggesting some sort of tidal streamer. These patches emit most strongly in the velocity range -110 to -130 km s^{-1} , that is, within about 50 to 70 km s^{-1} of the systemic velocity of M33, -179 km s^{-1} . The characteristic velocity of Wright’s cloud differs from the systemic velocity of M33 by about the same amount that the velocity of the M31 Cloud differs from the systemic velocity of M31.

5.2. The Local Group Ensemble of HVCs



hvc_m31_m33_wide_bv 3-OCT-1997 16:12 dip hartmann

Fig. 6.— HI emission integrated over the broad velocity range $-445 \leq v_{\text{LSR}} \leq -85 \text{ km s}^{-1}$ in the general vicinity of M31 and M33. Wright’s cloud is the extended hook-shaped HVC patch centered near $l = 128^\circ$, $b = -33^\circ$. M31 and M33 both appear larger here than in Figure 5 because the larger velocity range incorporates more of the gas from the disks of these galaxies; similarly, several additional HVCs are seen in this figure but not in Figure 5.

5.2.1. Spatial Distribution

We have so far established that at least one HVC is extragalactic, and that there are a number of HVCs plausibly associated with the most massive members of the Local Group. All of the emission seen in Figure 6 at $b < -15^\circ$, with the exception of that from the disks of M31 and M33, is contributed by HVCs, suggesting that the entire region is replete with these objects. Figure 7 shows the high-velocity emission from a larger region of the LD survey, $210^\circ > l > 90^\circ$, $-5^\circ > b > -65^\circ$, centered approximately on the direction of the barycenter of the Local Group. Emission from the gaseous disk of the Milky Way is seen as the band running along the top of the image from $l = 90^\circ$ to 160° . All of the remaining emission is due to HVCs. Some of the smaller HVCs pervading this larger region are not catalogued by WvW91 because of the more complete spatial sampling of the LD survey.

HVCs are not uniformly distributed on the sky, and Wakker’s (1991) Figure 2, (reproduced here as Figure 8), demonstrates this well-known, important point.

The figure shows HI column-density contours of the HVCs catalogued through 1990. Wakker identifies 10 distinct populations but, for the purposes of our discussion, identification of four major HVC groupings suffices to encompass most of the HVCs over the entire sky. These are: (1) the Magellanic Stream (indicated by MS in Figure 8); (2) the Northern Hemisphere Clouds ($210^\circ > l > 60^\circ$; $70^\circ > b > 30^\circ$) comprising Complexes A, C, and M); (3) the Local-Group Barycenter Clouds ($210^\circ > l > 90^\circ$; $10^\circ > b > -60^\circ$) comprising Complexes G, H, and ACHV; and (4) the Local-Group Antibarycenter Clouds ($310^\circ > l > 210^\circ$; $50^\circ > b > 10^\circ$) comprising the HVC Complexes WA, WB, WC, and WD discovered by Wannier & Wrixon (1972) and Wannier, Wrixon, & Wilson (1972) at moderate positive-velocity deviation values, and the EP clouds (see references in WvW91) at extreme positive-velocity deviations.

Each of these major groupings of HVCs has a distinct kinematic signature. The Magellanic Stream is a narrow streamer running through the South Galactic Pole and the Magellanic Clouds, and is contiguous over hundreds of degrees on the sky over a wide range of velocities. The Northern Hemisphere Clouds are also contiguous in space and velocity, but the clouds have a narrower velocity extent than the MS. These clouds, which are the most extensively studied of all HVC groupings, all have negative velocities, with velocities traceable into the IVC regime or even into the regime of conventional Galactic-disk kinematics. The Local-Group Barycenter Clouds comprise the clouds seen in the general direction of the massive Local Group galaxies, and all have negative velocities relative to the LSR. The Local-Group Antibarycenter Clouds all have positive velocities relative to the LSR. The clouds constituting this grouping are situated approximately opposite to the direction of the barycenter of the Local Group. They do not form well-defined streamers: the

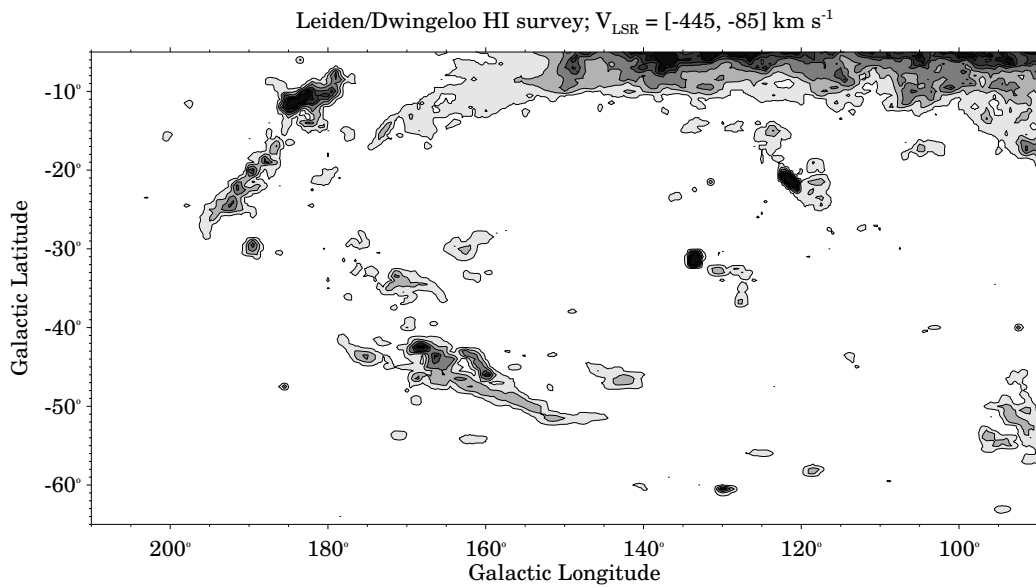


Fig. 7.— HVCs seen over an extended range of latitude and longitude, approximately centered on the direction of the barycenter of the Local Group, and emitting in the same velocity range as represented in Figure 6. The band running along the top of the figure to $l \simeq 160^\circ$ represents conventional-velocity HI emission from the gaseous disk of the Milky Way. The entire region is replete with HVCs: the WvW91 compilation tabulates some 100 individual clouds within the boundaries of this figure.

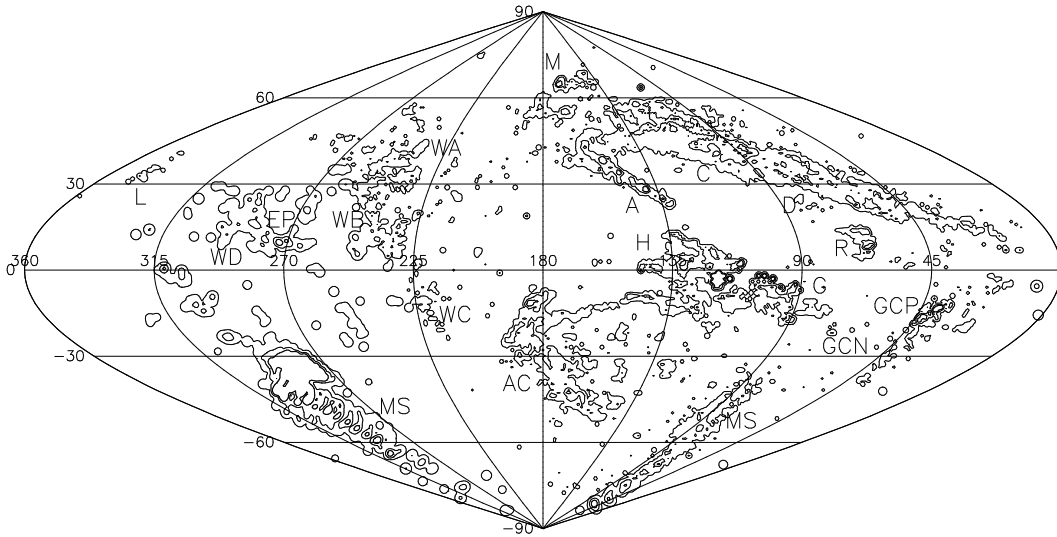


Fig. 8.— Reproduction of Wakker’s (1991) Figure 2, in a somewhat different projection, showing the locations of HVCs on the sky. Individual HVC complexes are contoured by column density and labeled according to Wakker’s nomenclature; the principal groupings are described in the text in the context of the Local-Group hypothesis. In general, clouds with $l \leq 180^\circ$ have negative LSR velocities; those with $l \geq 180^\circ$, positive LSR velocities.

individual members of this grouping are spatially distinct, relatively small in extent, and with modest kinematic gradients. Unlike the Northern Hemisphere Clouds, both the Barycenter and the Antibarycenter groupings are characterized by clouds with radial velocities that vary greatly from cloud to cloud over the spatial extent of the entire grouping. In what follows, we eliminate the Magellanic Stream clouds from the statistics of the HVCs, because their origin is known and is evidently distinct from that of the other clouds.

5.2.2. *Kinematics of the Individual Groupings*

We consider first the Local-Group Barycenter Clouds. An estimate of the positional centroid of this grouping from Figures 7 and 8 yields $l = -143^\circ$, $b = -23^\circ$. This centroid is remarkably close to the projected barycenter of the Local Group calculated by Einasto & Lynden-Bell (1982) to be at $l = 147^\circ$, $b = -25^\circ$, and well within the error ellipse of their estimate. The angular extent of the Barycenter grouping is approximately a steradian, roughly what one would expect if the volume of the Local Group were filled with these clouds. But if these clouds are related to the Local Group, they must then share its kinematics. The mean velocity, velocity extent, and the velocity centroid of the ensemble of HVCs provide a good test of which frame of reference is most relevant.

Imagine a frame of reference moving at constant velocity relative to the barycenter of a group of objects such as the HVCs. In this moving frame, the mean velocity of the ensemble will be shifted, but the velocity dispersion will remain unchanged. On the other hand, in a reference frame that is rotating with respect to the barycenter of the ensemble and offset from it, the observed velocity dispersion will be increased; there may be also be a shift in the mean velocity, depending on the distribution of the ensemble on the sky, although such a shift would tend toward zero for full-sky coverage. Consider, for example, the radial velocities of globular clusters relative to the local standard of rest and relative to the Galactic-center standard of rest (GSR). Clearly, the velocity dispersion of the ensemble of globular clusters should be smaller when measured relative to the GSR, and there would be no shift in the mean velocity. Transformation from LSR to GSR coordinates is achieved by subtracting the motion of the LSR, $220 \sin l \cos b \text{ km s}^{-1}$, from the LSR velocity of each globular cluster. Using the compilation of Harris (1996), we find that the globular clusters have a dispersion of 134 km s^{-1} and a mean velocity of $9 \pm 12 \text{ km s}^{-1}$ relative to the LSR; relative to the GSR, the dispersion is 119 km s^{-1} with a mean of $3 \pm 11 \text{ km s}^{-1}$, as expected.

If we now consider the system of HVCs in the same way, the change in the velocity dispersion is even more dramatic; the results are shown in Figure 9. The dispersion of the complete HVC ensemble is 159 km s^{-1} relative to the LSR; relative to the GSR, it falls to 101

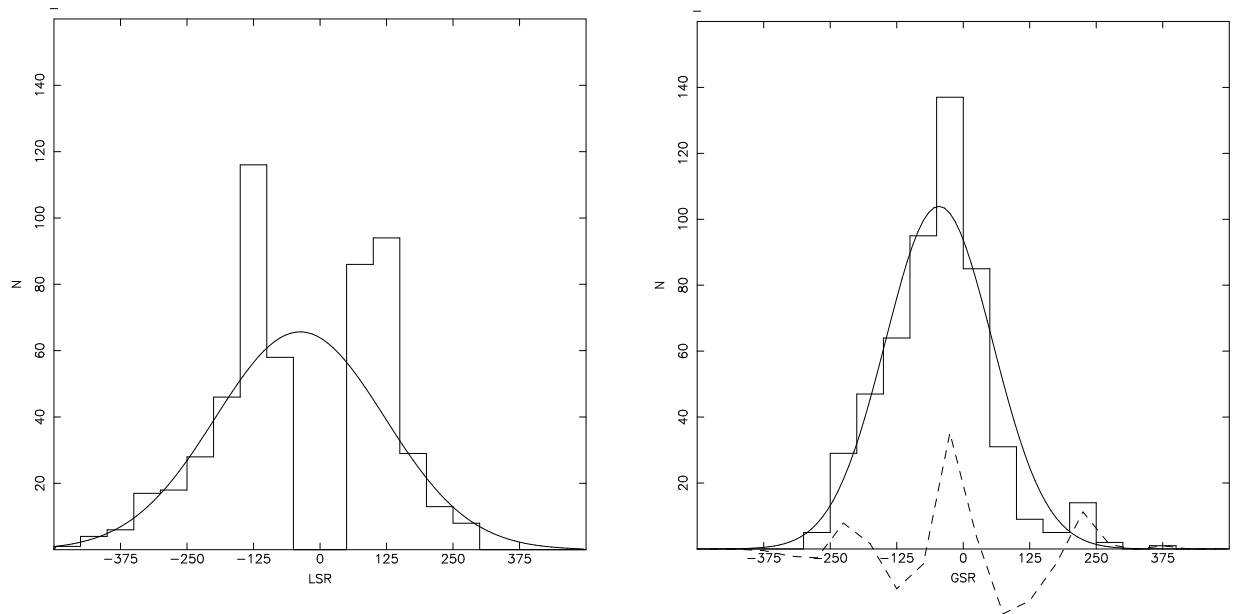


Fig. 9.— *Left:* Histogram of the distribution of HVC velocities relative to the LSR. HVCs which might in fact have v_{LSR} near zero are not plotted, because such clouds would not be separable from conventional-velocity Galactic emission. *Right:* Distribution of HVC velocities relative to the GSR. A Gaussian profile was fit to the wings of both histograms: the v_{GSR} distribution of the HVCs is more narrowly confined than the v_{LSR} one, suggesting, as discussed in the text, that the GSR system is the more relevant reference frame. The data in both panels are from the WvW91 catalogue of HVCs.

km s^{-1} . The mean velocity in both cases is, however, significantly different from zero: $-37 \pm 7 \text{ km s}^{-1}$, measured with respect to the LSR, and $-46 \pm 4 \text{ km s}^{-1}$ measured with respect to the GSR. These values suggest that the GSR inertial frame is more appropriate than the LSR frame, and that both the GSR and LSR frames are moving at constant velocity relative to the barycenter of the HVCs. This result is at variance with a Galactic origin for the HVCs. If HVCs originated in the Galactic disk, then the velocity dispersion of the HVC ensemble would be lower in the LSR frame because the gas would conserve angular momentum. If the HVCs originated in the Galactic center, the mean velocity of the ensemble would be zero. Evidently, the entire Milky Way is moving toward the barycenter of the HVCs.

If so, then the velocity centroid of the Local Group Barycenter Clouds should reflect the motion of the Milky Way toward the Local Group barycenter, which is given by Einasto & Lynden-Bell (1982) as -82 km s^{-1} relative to the LSR. We define the Barycenter Clouds as all of the HVCs within an ellipse centered on $l = -143^\circ$, $b = -23^\circ$, with a major and minor axis of 60° and 30° , respectively, and where the major axis is tilted by 30° counterclockwise from $b = 0^\circ$. Some 96 of the clouds catalogued by WvW91 fall within this ellipse. Relative to the LSR, the mean velocity of these clouds is $-173 \pm 10 \text{ km s}^{-1}$; relative to the GSR, the mean velocity is $-88 \pm 11 \text{ km s}^{-1}$. If we now subtract the motion of the GSR relative to the Local-Group Standard of Rest (LGSR), the mean velocity of the Local-Group Barycenter Clouds becomes $-28 \pm 10 \text{ km s}^{-1}$, suggesting that the LGSR is a reference frame more appropriate to the Local-Group Barycenter Clouds than either the GSR or the LSR reference frames.

We note, however, that although the change of coordinate systems produces a considerable lowering of the mean velocity of the Local-Group Barycenter HVCs, the mean is still marginally negative. Furthermore, the Antibarycenter Clouds, which are on the opposite side of the Milky Way from M31, also have a negative mean velocity relative to the GSR and to the LGSR of $-57 \pm 12 \text{ km s}^{-1}$ and $-124 \pm 12 \text{ km s}^{-1}$, respectively. It is reasonable to ask why reduction to the LGSR does not produce a zero mean velocity if it is the non-translating inertial reference frame, and, furthermore, why the clouds that are approximately opposite on the sky to the Barycenter Clouds are moving more rapidly toward the barycenter of the Local Group than the Barycenter Clouds themselves. We note in this regard that a non-zero mean velocity of the HVCs relative to the barycenter would occur if the entire cloud ensemble were either expanding or contracting; a negative mean velocity implies infall, as first accounted for in the model of Bajaja et al. (1987). Second, if the Milky Way is itself falling toward the barycenter of the Local Group as postulated by Kahn & Woltjer (1959), because the Milky Way lies between the Antibarycenter Clouds and the barycenter, the Antibarycenter Clouds would be accelerated both toward the Milky Way *and* toward the barycenter of the Local Group, with the sign and relative magnitude consistent with the observed mean radial velocities. In § 6, we discuss a model for the dynamics of

the HVCs in the Local Group that reproduces the observed negative mean LGSR velocities in both the Barycenter and Antibarycenter cloud groupings. In this model, the HVCs are fragments remaining from the (continuing) formation of the Local Group, falling towards its center of gravity.

5.2.3. *Velocity Extrema*

No cloud is catalogued in the WvW91 compilation with a positive velocity higher than $v_{\text{LSR}} = 297 \text{ km s}^{-1}$, and no cloud with a negative velocity lower than -464 km s^{-1} , even though the useful velocity range of the principal surveys contributing to that catalogue is -900 to $+800 \text{ km s}^{-1}$. This limitation on the velocity extent of the HVC ensemble suggests that the HVCs constitute a gravitationally bound system of clouds rather than a collection of objects more or less randomly distributed in extragalactic space, which would not show such cutoff velocities.

One cannot use either the value of the velocity dispersion or the values of the velocity extrema to differentiate between a Galactic and an extragalactic origin, because both origins encompass the observed values, but it is reasonable to ask what sort of mass would keep the clouds bound in the Local Group hypothesis. For a radius of 1.5 Mpc, (see §6 below) the measured one-dimensional velocity dispersion of 106 km s^{-1} gives a mass of $2.1 \times 10^{12} M_{\odot}$ for a virialized ensemble of objects. This mass is close to the mass of $3.0 \times 10^{12} M_{\odot}$ obtained from the timing argument by Kahn & Woltjer (1959).

5.2.4. *Angular-Size/Velocity Relation*

Imagine that all of the HVCs (again excluding the Magellanic Stream) comprise a single class of extragalactic objects. If the clouds have a uniform set of properties, such as a single power-law size distribution independent of their location in the Local Group, then the nearer clouds would have, on average, a larger angular extent than the more distant ones. In that case, it should be possible to distinguish kinematically the nearer clouds from the more distant ones. We note first that most of the luminous mass in the Local Group is concentrated in M31 and the Milky Way, and that these two galaxies are approaching each other at a velocity of 123 km s^{-1} . Relative to the GSR, one would then expect that the clouds closest to the Milky Way would have velocities closest to 0 km s^{-1} . If the HVCs are falling toward the Local Group barycenter, then those clouds with the most negative velocities with respect to the GSR would be the most distant; in the terms of the present

analysis, these would correspond to clouds on the far side of M31, approaching both M31 *and* the barycenter. Increasing distance would correspond roughly to increasingly negative velocity with respect to the GSR. We therefore would expect a significant correlation between angular size and GSR velocity.

The angular size, Ω , tabulated by WvW91, plotted against GSR velocity, with clouds collected in bins 50 km s^{-1} wide, is shown in Figure 10. The error bars give the statistical uncertainty of the mean in each bin. Except for the highest positive velocities (which represent very few clouds in any case), there is a good correlation between angular size and GSR velocity in just the sense expected if the HVCs were associated with the Local Group. The slope of the distribution depends in detail on the dynamics of the Local Group, the distribution of HVC sizes, and the trajectories of the individual clouds, as discussed in some additional detail below. It is difficult to see how a Galactic origin for the HVCs could produce this correlation; there is no such correlation in a plot of Ω versus v_{LSR} .

6. Local Group Dynamics

6.1. Cosmological Background

The continuing accretion of gas and dark matter onto galaxies and groups is an inevitable prediction of all hierarchical models of the formation of structure in the Universe. According to these models, gravitational fluctuations in the dark matter first collapse to form small, bound objects. If the velocity dispersion in these “mini-halos” exceeds 10 km s^{-1} , then they are able to accumulate baryons (Ikeuchi 1986; Rees 1986; Bond, Szalay, & Silk 1988; Babul & Rees 1992; Miralda-Escude & Rees 1993; Kepner, Babul, & Spergel 1997). These mini-halos will collect into filaments; those nearby would then fall onto the Local Group, resulting in an accretion shock at the edge of the Local Group.

Outside this shock, the gas and dark matter in the mini-halos would likely move together as the clouds fall onto the Milky Way. It is not clear whether the gas and dark matter will be separated at the accretion shock or whether a cloud will survive ram-pressure stripping; it is also not clear whether tidal forces will destroy the mini-halos. The subsequent evolution of the clouds (once they are imbedded in a hot intragroup medium) will depend on things such as the rate of evaporative heating (which depends on unknowns such as the magnetic field structure). The fate of the dark matter will depend upon the mean density in these small halos.

The location of most of the baryons in the local universe is not known, but it is reasonable to suspect that they are associated with the mini-halos which are collected into the filaments

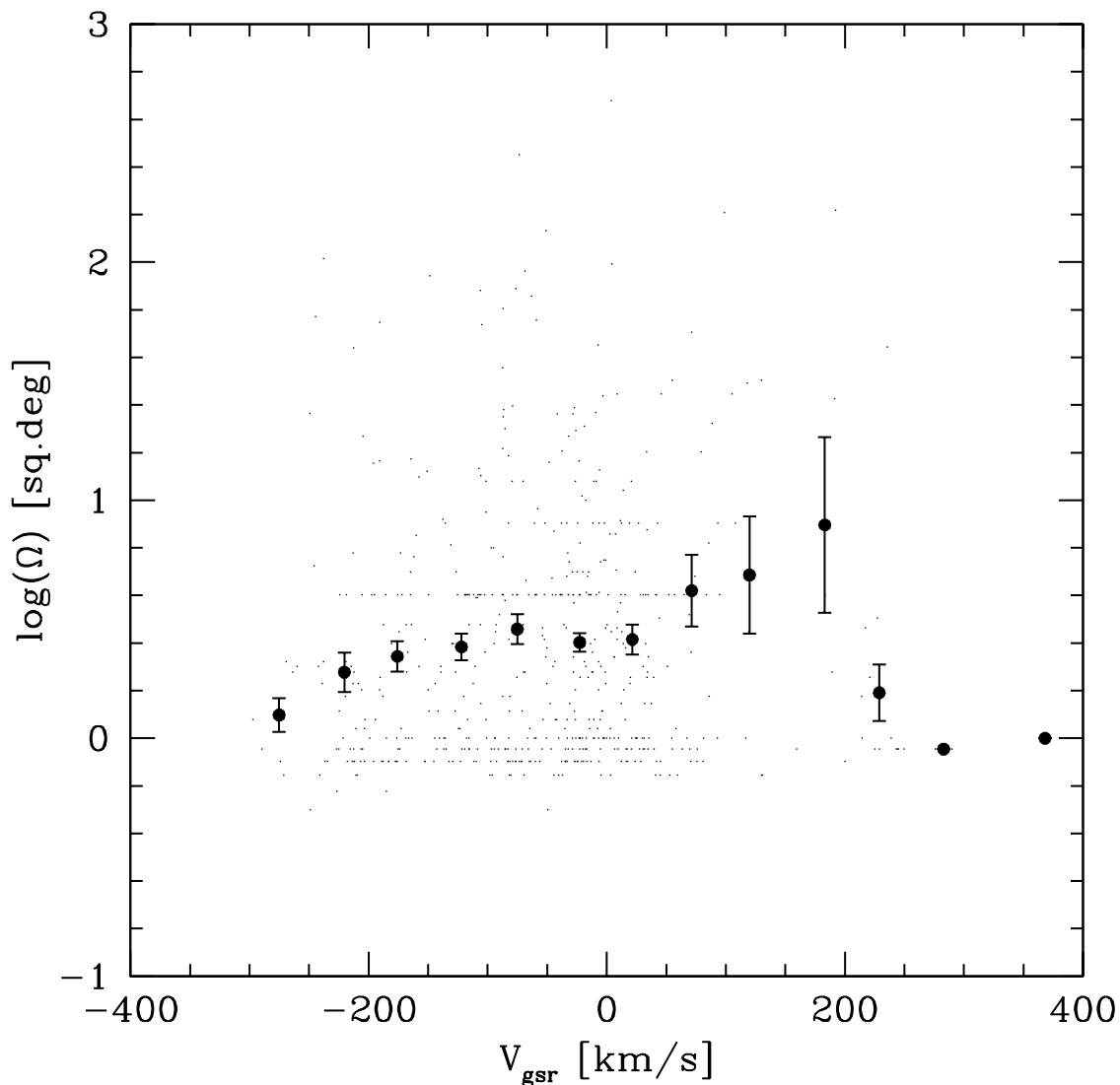


Fig. 10.— Variation of angular size with respect to GSR velocity for the HVCs in the WvW91 catalogue. Individual clouds are shown as small dots; the large dots represent the material averaged over bins 50 km s^{-1} wide. The error bars represent $\pm\sqrt{N-1}$ uncertainties; bins without such bars represent only a single point. The apparent quantification at low values of Ω reflects the finite sampling of the data in WvW91. HVCs with very negative values of v_{GSR} tend to have smaller angular sizes.

and sheets around galaxy clusters. Measurements of the deuterium abundance (Tytler, Fan, & Burles 1996) suggest that $\Omega_b h^2 \simeq 0.025$ at the epoch of nucleosynthesis. Analyses of the Lyman- α forest (Rauch et al. 1997) infer a lower limit on baryon abundance in cold gas of $\Omega_b h^2 > 0.023$. There is little cold gas seen in absorption at low redshifts, however, and the local stellar density, $\Omega_* h^2$, is only 0.007 (Fukugita et al. 1997). Numerical simulations (Cen et al. 1995) suggest that much of the gas is in filaments and sheets, where it has not yet been detected.

While most of the gas in the filaments would be ionized, some of it may be neutral. The Lyman- α forest and the Lyman-limit systems trace the distribution of this neutral gas on cosmological scales (McGill 1990; Cen et al. 1994; Zhang, Annios, & Norman 1995; Hernquist et al. 1996; Miralda-Escude et al. 1996; Bi & Davidsen 1997; Bond & Wadsley 1997). We suggest in this paper that Galactic astronomers have been observing the same type of gas clouds and identifying them as HVCs.

The Local Group is probably a dynamically young system, with the Milky Way and M31 approaching each other for the first time. Hierarchical models suggest that there is continuing accretion of gas onto the Local Group through filaments. While most of this gas is likely to be ionized, there would be neutral gas that is able to cool when higher densities are reached in dark-matter mini-halos. In such a situation, there would be small, neutral, gas clouds with velocity dispersions of $\sim 10 \text{ km s}^{-1}$ embedded in the large, coherent, velocity fields of the filaments. These filaments would contain mass comparable to the total mass in the Local Group.

The dynamics of the Local Group is probably rather simple: more than 98% of the mass of the Local Group is contributed by M31 and its satellites and by the Milky Way and its satellites (Raychaudhury & Lynden-Bell 1989, hereafter RL). Thus the dynamics of the Local Group can be approximated as a two-body problem, with M31 and the Milky Way approaching each other on nearly radial orbits (Einasto & Lynden-Bell 1982).

The gravitational effects of neighboring galaxies complicates this simple two-body interaction. The neighboring galaxies exert a net force on the Local-Group barycenter that produces a bulk flow of the entire Local Group and, in addition, exert a tidal force that compresses and shears the Local Group. While the bulk flow is probably primarily due to distant mass concentrations such as the Great Attractor and the Coma Cluster, the tidal force is primarily due to neighboring galaxies. RL estimate the tidal field from samples of nearby galaxies. The effect of the Local Group neighbors is to compress the flow of material in one dimension and to shear it along an axis that is not far from the line joining M31 and the Milky Way.

6.2. Simulating the Dynamics of the HVCs

We have done a simple simulation of the formation and evolution of the Local Group. The dynamics are approximated as a modified restricted three-body problem. The test particles in the simulation are subject to the gravitational forces of M31 and the Milky Way, and to the external tidal field of the neighboring galaxies. We use the model of RL to simulate the external tidal field and its temporal evolution (see their Table 5). For these parameters, M31 today has a tangential velocity of 38 km s^{-1} and the typical galaxy is assumed to have a mass-to-light ratio of 66. (We also ran a simulation for a mass-to-light ratio of 80, but the results do not differ significantly from those discussed below.)

The simulation begins when the physical distance between M31 and the Milky Way is 0.1 Mpc. We represent M31 and the Milky Way as “sticky particles”, assigning one third of the Local Group mass to the Milky Way and the remaining two thirds to M31. Any test particle that is falling towards the two galaxies and passes within 100 co-moving kpc of their centers is assumed to be accreted onto the galaxies.

The net effect of the external tidal field and the gravitational pulls of M31 and the Milky Way is to compress most of the test particles into a filament. This can be seen in Figure 11, which shows the (x, y) and (x, z) projections of the test-particle density in the simulation, and in Figure 12, which shows the velocity field. We identify the test particles remaining at the end of the simulation with the HVCs. Today, $\sim 25\%$ of the mass in the simulation would be bound to the Milky Way, and $\sim 50\%$ to M31; the remaining mass would still remain in the filament. If the known HVCs have distances similar to those implied by the simulation, the total mass of the remaining neutral hydrogen is $\sim 10^{11} M_{\odot}$.

The simulated velocity field shown in Figure 12 suggests that the gas flow along the filament is smooth and likely cold to the “left” of the Milky Way and to the “right” of M31. In the region between M31 and the Galaxy, the streamlines cross; such a situation would likely produce shocks, suggesting that M31 and the Milky Way could be imbedded in a common halo of hot gas. In the simulation, we bin the particles into $0.1 \times 0.1 \times 0.1 \text{ Mpc}^3$ cubes and compute density, velocity, and velocity moments in each cube. Whenever $\langle v^2 \rangle$ in a cube exceeds $(100 \text{ km s}^{-1})^2$, the gas in the cube is assumed to be hot.

Figure 13 shows that the tidal and gravitational fields have compressed most of the gas into a large filament that stretches from $l = 120^{\circ}$, $b = -10^{\circ}$ to $l = 300^{\circ}$, $b = 10^{\circ}$. This orientation is due to two effects: the M31/Milky Way axis lies along a line through $l = 122^{\circ}$, $b = -21^{\circ}$ and the tidal stretching by the external galaxies lies along an axis pointing toward $l = 143^{\circ}$, $b = -23^{\circ}$. The lower panel in Figure 13 represents only the cold gas. The morphology of the simulated particles does not depend sensitively on the removal of the hot

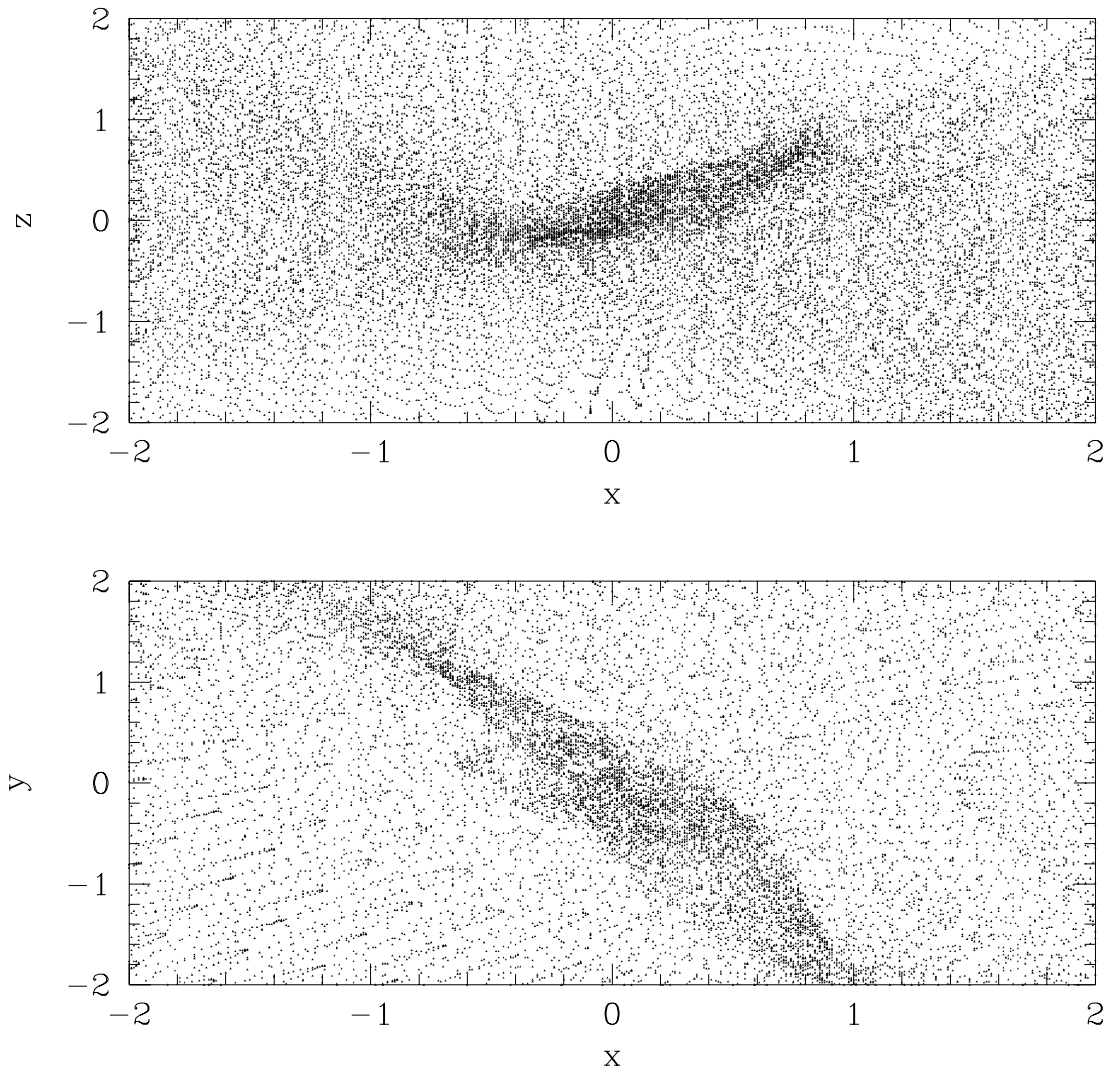


Fig. 11.— Locations of the simulated HVC particles at the termination of the simulation described in the text. The upper panel shows the (x, z) projection; the lower panel shows the (x, y) one. Distances are given in Mpc. The Milky Way is located at $(0.23, -0.38, 0.18)$; M31, at $(-0.12, 0.19, 0.09)$. Any test particle that fell inwards towards the two galaxies and passed within 100 co-moving kpc of their centers was assumed to be accreted onto the galaxies and was excluded from this plot and the subsequent discussion.

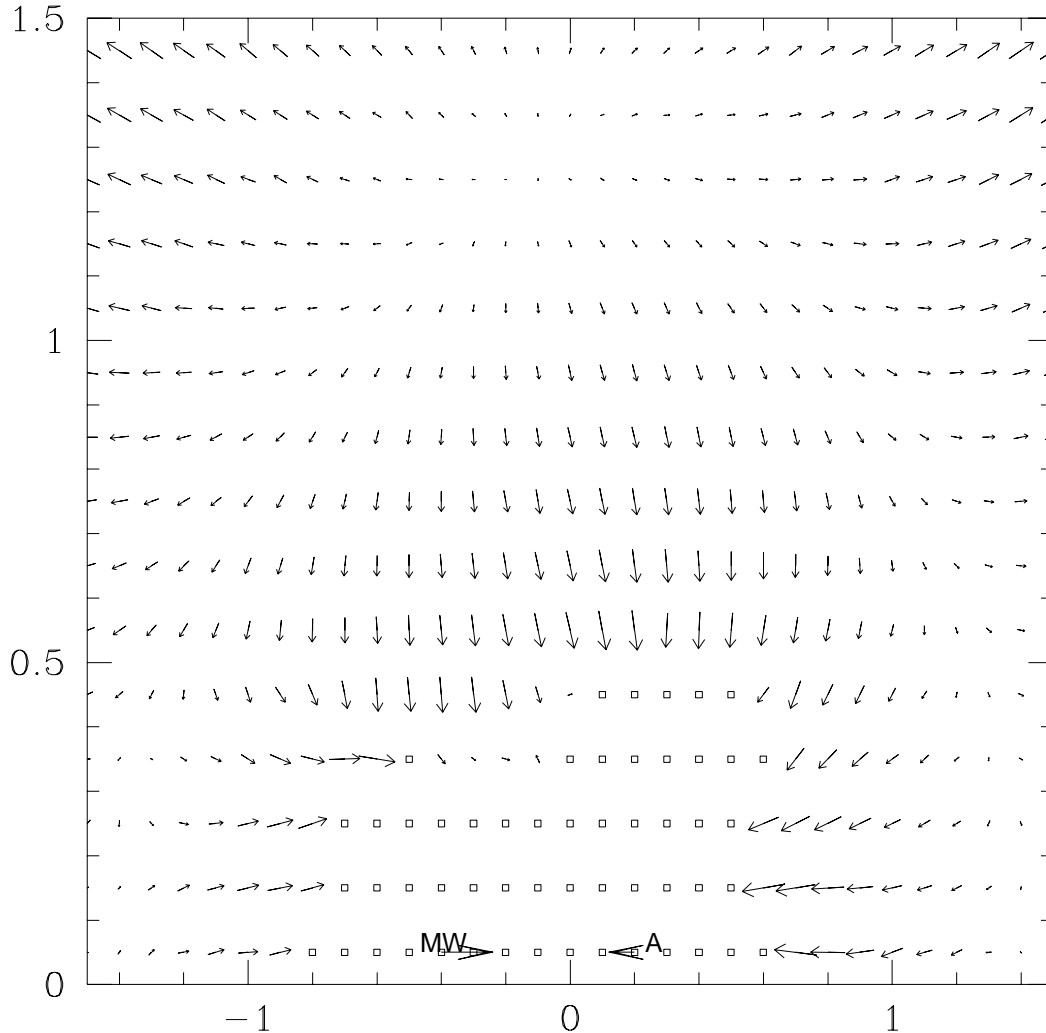


Fig. 12.— Simulated velocity flow in the Local-Group rest frame. The Milky Way and M31 (marked by MW and A, respectively) are moving towards each other with relative velocity 124 km s^{-1} . Their gravitational pull, together with the external tidal field, produces flow towards a filament (see the vectors above the plane). Material in the filament (and near the Local Group) flows along the filament as indicated; material beyond the Local-Group accretion radius partakes in the general Hubble flow. The squares show regions where the gas random velocity (computed with a 100 kpc smoothing length) exceeds $(100 \text{ km s}^{-1})^2$: this gas is likely shock heated. The distance at which the Hubble flow is reversed is about 1.5 Mpc.

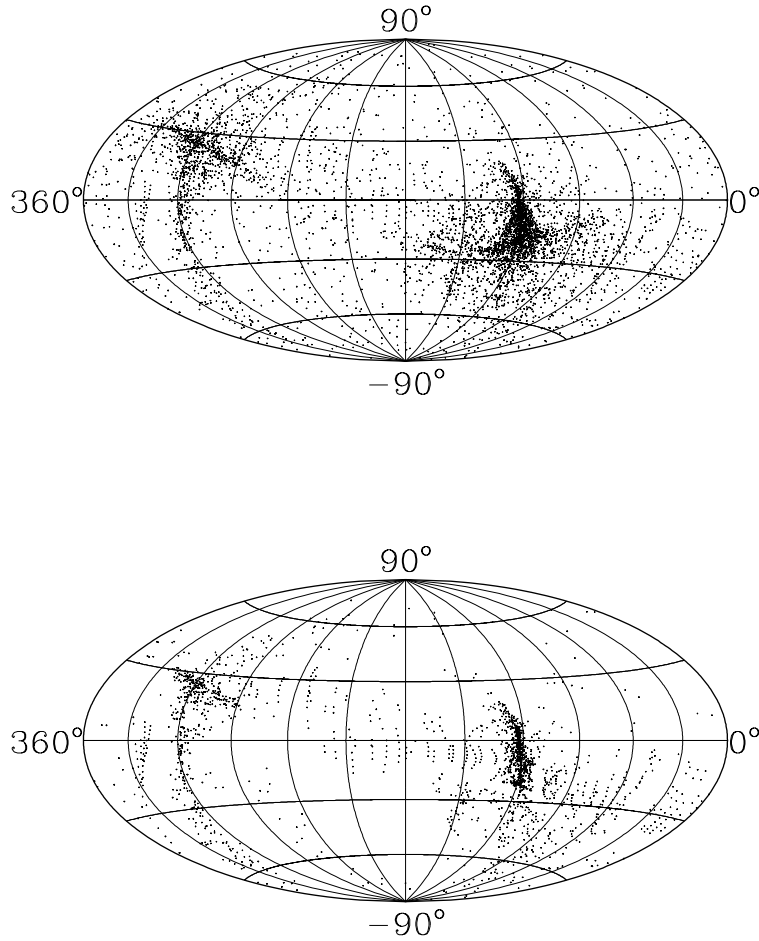


Fig. 13.— Distributions on the sky of the simulated HVC particles, calculated for two values of the velocity dispersion within the 100-kpc smoothing box. *Upper*: Projection showing all of the test particles within 2 Mpc of the Milky Way, regardless of the velocity dispersion. *Lower*: Same projection as in the upper panel but here showing only those particles located in regions in which the gas random velocity within the 100-kpc smoothing box is less than $(100 \text{ km s}^{-1})^2$. The overall distribution on the sky is similar in both cases.

gas.

6.3. Comparison with the HVC Observations

We estimate the column density associated with the simulated Local–Group HVCs by binning the particles in l, b, v space and then integrating the total column at each grid point. We assume that $\Omega_b/\Omega_{\text{tot}} = 0.1$ and that all of the overdensity in the Local Group region is already bound to M31 and to the Milky Way. By restricting our analysis to gas that has not yet passed through the Local Group accretion shock, we exclude any nearby gas. It is not clear that this is a valid restriction, as some of the gas clouds may in fact survive passage through this shock. However, the similarity in the spatial distributions shown in the two panels of Figure 13 suggests that inclusion or removal of the hot gas should not strongly affect the comparison of the simulation with the observations. Accordingly, the upper panel in Figure 14 shows *all* of the regions with the same velocity and column density criteria, and thus represents the HVCs in the simulation. The larger symbols correspond to regions of higher column density in the simulation.

We now compare the simulated results shown in the upper panel of Figure 14 with the observations. We first remove from the observations the HVCs constituting the Magellanic Stream as well as the grouping of Northern Hemisphere Clouds and plot the results in the lower panel of Figure 14; positive and negative LSR velocities are indicated separately. Direct distance measurements (Danly et al. 1993; van Woerden et al. 1997) indicate that the Northern Hemisphere Clouds are relatively nearby and thus would distort the overall statistical comparison. The agreement with the observations of the simulated spatial distribution, velocity separation, and direction of the HVC velocities is rather good, considering the simplicity of the model.

We next compare the observed and simulated longitude–velocity distributions of the HVCs in the LSR frame. Figure 15 shows several features well represented in the simulation. The envelope of the observed velocities is approximately sinusoidal, but is displaced from $v_{\text{LSR}} = 0 \text{ km s}^{-1}$ by about -100 km s^{-1} . Both the functional form of the envelope and the displacement from zero (due in part to the motion of the LSR toward the barycenter of the Local Group) are reproduced in the simulation. Furthermore, the amplitude of the envelope is reproduced. Certain details, such as the negative–velocity HVC gas between $180^\circ > l > 205^\circ$ and at $l > 340^\circ$ are also accounted for by the simulation.

The Local–Group hypothesis thus is able to account for important aspects of the spatial and of the kinematic distributions of HVCs. The model is simple, and rather insensitive to

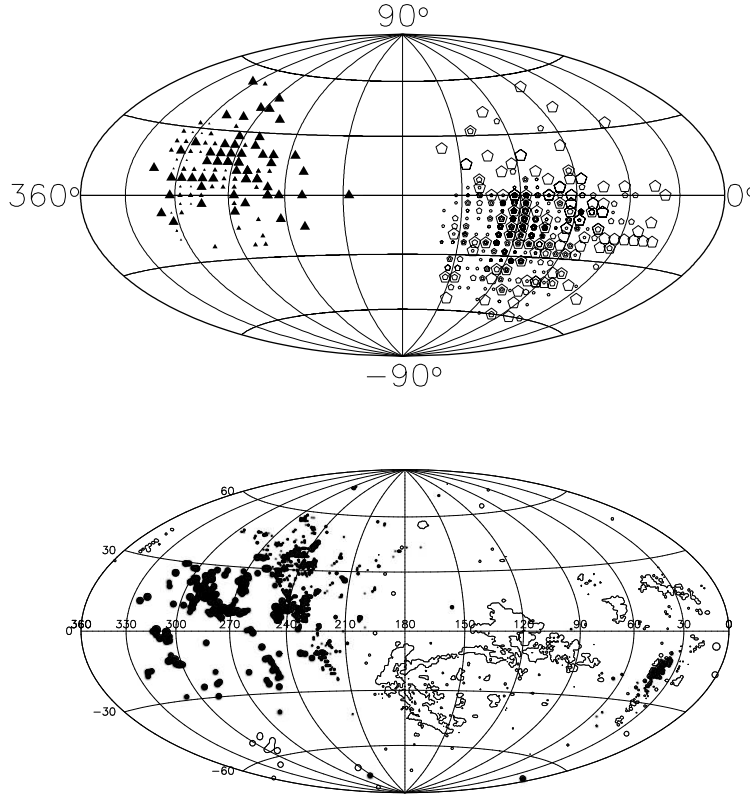


Fig. 14.— Comparison of simulated and observed sky- and kinematic distributions of the HVC ensemble. *Upper:* Distribution of all simulated clouds having HI column densities greater than $3 \times 10^{18} \text{ cm}^{-2}$ and $|v_{\text{LSR}}|$ greater than 200 km s^{-1} , regardless of the dispersion within the smoothing box. The small, medium, and large symbols denote, respectively, simulated clouds with column densities between 3×10^{18} and 1×10^{19} , between 1×10^{19} and 3×10^{19} , and greater than $3 \times 10^{19} \text{ cm}^{-2}$. Strictly speaking, these simulated column densities are total ones, i.e. including the dark-matter content. The triangles represent clouds with negative velocities; the stars, clouds with positive velocities. This figure represents the distribution of HVCs if the clouds have not been destroyed by passage through a hot intergalactic medium and if collisions between HVCs are rare. *Lower:* Distribution of observed HVCs, as in Figure 8 in Aitoff projection, but excluding the Magellanic Stream and the Northern Hemisphere Complexes A, C, and M, which are evidently relatively nearby and thus unrepresentative of the angular size of individual clouds in the Local-Group ensemble. Positive velocities are denoted by filled contours, negative velocities by open contours. The simulated spatial and kinematic distributions resemble, in essence, the observed distributions. The lower panel was kindly provided by Bart Wakker.

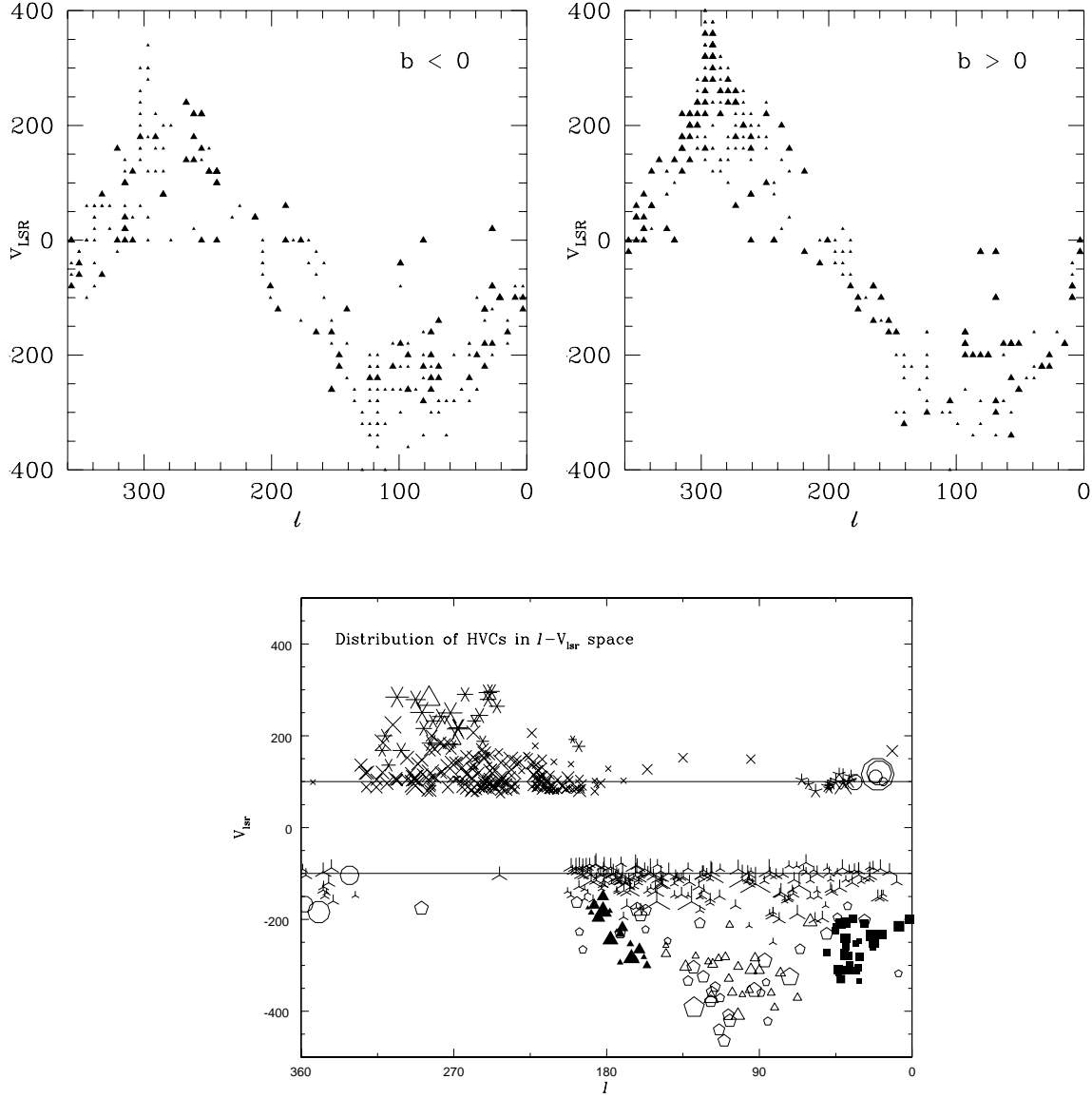


Fig. 15.— Comparison of the simulated longitude–velocity distribution of the HVCs with the observed situation. Radial velocities are relative to the LSR. *Upper:* Simulated kinematic distribution of clouds with HI column densities greater than $3 \times 10^{18} \text{ cm}^{-2}$, plotted separately for $b < 0^\circ$ and for $b > 0^\circ$. *Lower:* Longitude–velocity diagram of the observed HVC ensemble, as compiled by WvW91. The symbols are proportional in size to the flux from the individual clouds, and are keyed to the individual complexes defined by Wakker (1991). Clouds with LSR velocities $|v_{\text{LSR}}| < 80 \text{ km s}^{-1}$ are not considered here as HVCs, regardless of their location. The general features observed are accounted for by the simulation.

the tunable parameters. It suggests identifying HVCs as the structures from which the Milky Way and M31 have been built, and which fuel the continuing star formation in both galaxies. It further suggests that the HVCs are among the first structures to form in the Local Group, and that these clouds can be expected to be associated with copious dark matter.

6.4. Lyman- α Clouds

The simulation suggests that the Local Group is similar to other galaxy groups which have been numerically modeled. In numerical simulations of the formation of large-scale structure, most galaxies and groups are in filaments (e.g. Hernquist et al. 1996; Bond, Kofman, & Pososyan 1995). Within these filaments, hot gas is associated with individual groups. Outside the groups, the gas is primarily cold. This cold filament gas seems to have properties similar to those of the Lyman- α forest and Lyman-limit lines observed in absorption toward distant quasars (see e.g. Hernquist et al. 1996 and Katz et al. 1996).

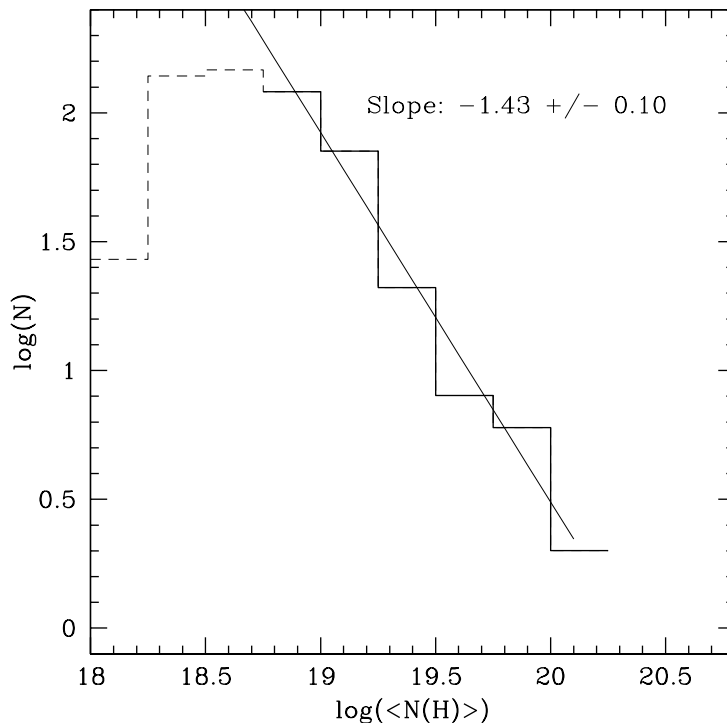


Fig. 16.— Histogram of the mean column-density distribution of the HVCs from the WvW91 compilation. The straight line fits the data at the higher column densities, $N_{\text{HI}} > 3 \times 10^{18} \text{ cm}^{-2}$, for which the sample is likely complete.

The mini-halos may account for the core-halo structure seen in some of the HVCs

(Giovanelli, Verschuur, & Cram 1973; Cram & Giovanelli 1976; Giovanelli & Haynes 1977; Wakker & Schwarz 1991; Wolfire et al. 1995). When the ionization rate is not high enough to balance cooling, there is an instability that enables cold gas to accumulate in the center of the halo (Murakami & Ikeuchi 1990; Kepner et al. 1997). Over a wide range of parameters, this cold gas is primarily atomic rather than molecular. In this picture, the HVCs are gravitationally bound by the dark matter rather than pressure confined (see e.g. Wolfire et al. 1995). Because this instability may lead to some star formation (Murakami & Ikeuchi 1990), it would be intriguing to see if there are ultra-low-surface-brightness galaxies associated with some of the HVCs.

If the formation of the Local Group is typical of the formation of small groups, and if HVCs are indeed the leftover building blocks of local galaxy formation and evolution, similar objects would be expected in other galaxy groups. We speculate that the Ly- α clouds may be such systems and discuss them below; we discuss in §7.3 HVCs in emission toward other galaxies. The HVCs correspond to Lyman-limit systems in the column density range $2 \times 10^{17} \text{ cm}^{-2} < N_{\text{HI}} < 2 \times 10^{20} \text{ cm}^{-2}$. As can be seen from Figure 16, the HVCs span the middle of this range. Lower column densities correspond to clouds in the Ly- α forest; higher column densities correspond to damped Ly- α clouds.

Wolfe (1993) has plotted the frequency distribution of the full range of column densities detected in the Ly- α absorbers, showing that this distribution follows a power law with an index of -1.25 over the entire range of column densities and with an index of -1.67 for $\log N_{\text{HI}} > 20 \text{ cm}^{-2}$. That the power-law index of -1.4 ± 0.1 shown in Figure 16 is consistent with the index characterizing the Ly- α absorbers suggests that the HVCs may be manifestations of the same phenomenon. From a purely theoretical standpoint, the gas column densities associated with the dark matter mini-halos are expected to scale as $N_{\text{HI}}^{-5/3}$ (Rees 1988; Milgrom 1988), close to the value of the slope, -1.4 , seen in Figure 16. Thus, one of the expectations of our hypothesis is the existence of additional HVCs at lower column densities along the M31/Milky Way axis; these clouds may, however, be largely ionized.

We may roughly estimate the probability of detecting an HVC as a Ly- α absorber for an observer located external to the Local Group. The covering fraction of HVCs seen against a background quasar depends on column density and can be estimated from various observations. If the WvW91 catalogue is incomplete by a factor of 2 down to $N_{\text{HI}} = 1 \times 10^{18} \text{ cm}^{-2}$, then using the mean cloud properties within a Hubble-flow turnaround radius of 1.5 Mpc gives a covering fraction of 0.1, which is a value similar to that obtained by WvW91 if the Outer Arm Complex, Magellanic Stream, and Complex C are not included. Bowen, Blades, & Pettini (1995) estimate a covering fraction on the sky of 0.14 for $N_{\text{HI}} > 1 \times 10^{17} \text{ cm}^{-2}$ from HST GHRS spectra, a fraction which would be approximately doubled for an

external observer. Murphy, Lockman, & Savage (1995) obtain a higher value of the covering fraction, 0.37, for $N_{\text{HI}} > 7 \times 10^{17} \text{ cm}^{-2}$, but make no correction for the large clouds, which, to be consistent with the Bowen et al. estimate, would reduce the covering fraction to about 0.09, or 0.18 for an external observer, to the Murphy et al. sensitivity limit.

If HVCs are not randomly distributed within the Local Group, but show some concentration toward M31 and the Milky Way, then, extending the considerations to very distant systems, the probability of detection would be increased for a quasar within one or two hundred kpc of a host galaxy. One therefore expects a probability of about 0.3 for $N_{\text{HI}} > 1 \times 10^{17} \text{ cm}^{-2}$ at an impact parameter of 1.5 Mpc, and higher values at smaller impact parameters, depending on the degree of concentration at zero redshift. This probability might increase further for lower column densities, especially if the frequency distribution of low-column-density HVCs is similar to that of the Ly- α absorbers summarized by Wolfe (1993). Several ionized clouds without associated HI have, in fact, been detected in optical absorption lines toward BL Lac, as well as toward four extragalactic supernovae at velocities between -260 and $+263 \text{ km s}^{-1}$ (WvW97). One would expect a higher detection probability at higher redshifts, if the evolution of the HVC system is at all well described by our simulation (see §6.2). Hoffman et al. (1998) present Ly- α absorption data towards the quasar 3C 273, and show that the lowest-redshift absorber is located only ~ 200 kpc distant from the galaxy MCG+00-32-16, and at a velocity separation of only 94 km s^{-1} . They interpret this feature as due to a “failed dwarf” member of a poor galaxy group, i.e. as an HI cloud which has not formed stars; the properties of this cloud are compatible with those suggested here for HVCs.

7. Discussion

7.1. Distances

7.1.1. Absorption-Line Distances

The most obvious direct test of whether the HVCs are Galactic or extragalactic has involved searching for optical or UV absorption lines at the velocity of the HI emission toward sources at known distances. All but two of the attempts to find optical absorption lines toward stars in the halo of the Milky Way have returned negative results. Danly et al. (1993) and van Woerden et al. (1998) obtained distances toward Complexes M and A, respectively, of $1.7 < d < 5 \text{ kpc}$ and $4 < d < 10 \text{ kpc}$. These complexes have distances within the range expected for the Northern Hemisphere Clouds from the tidal considerations discussed in §4.2. In the Local-Group hypothesis, such distances are not representative of

the HVC ensemble as a whole because the two complexes are likely to be the nearest HVCs.

The HVC simulation and the cloud kinematics suggests that the mean HVC distance is ~ 1 Mpc, and that those clouds with the most negative radial velocities relative to the GSR in the general direction of M31 will be the most distant. We expect that it will be possible to obtain distances via stellar absorption lines only for the three HVC groupings with the largest angular sizes, namely for the Northern Hemisphere Clouds, the Magellanic Stream, and the Outer Arm Complex. The largest remaining clouds, including Complex H, might also be relatively nearby, compared to Local Group distances, with distances < 100 kpc. We would not, however, expect the small isolated clouds in the Barycenter or Antibarycenter groupings, with angular diameters ≤ 60 sq deg, to yield stellar absorption lines against stars in the Milky Way.

7.1.2. $H\alpha$ Distances

High-velocity clouds will be bathed by the interstellar radiation field leaking into the halo from the disk if they are Galactic, or by the intergalactic radiation field if they pervade the volume of the Local Group. In either case, the radiation field will ionize the outer envelope of neutral gas.

Recent observations of $H\alpha$ emission from HVCs place some limits on their distances (Kutyrev & Reynolds 1989; Songaila, Byrant, & Cowie 1989; Tufté et al. 1996; Weiner & Williams 1996; Tufté, Reynolds, & Haffner 1998; Weiner 1998). Weiner & Williams (1996) detected $H\alpha$ emission toward substructures in the Magellanic Stream at levels of 370, 210, and 200 mR (corresponding to emission measures, EM, of $0.5 - 1.0 \text{ cm}^{-6} \text{ pc}$), and attributed this emission to shock ionization because of the morphology of the emission. More recently, Tufté et al. (1998) detected $H\alpha$ emission along 13 lines of sight toward complexes A, C, and M at intensities ranging from 60 to 200 mR ($\text{EM} = 0.15 \text{ to } 0.5 \text{ cm}^{-6} \text{ pc}$). They attribute this emission to either ram-pressure shocks caused by the passage of the clouds through low density hot halo gas or to ionizing radiation leaking from the Galactic disk. The Magellanic Stream is at a distance of about 50 kpc and thus would be expected to have lower $H\alpha$ intensities than the nearer A, C, and M complexes, if both sets of clouds are photoionized. However, leakage radiation would depend weakly on distance from the plane as long as the Milky Way subtends a large angle as seen from the clouds, and would likely be non-uniform in the halo, which might explain the range and variation of observed intensities. On the other hand, if shock ionization is responsible for the emission from the A, C, and M complexes, the smaller $H\alpha$ intensities may be the result of lower velocities relative to the ambient halo gas than is the case for the Magellanic-Stream clouds. In any event, we expect most of the

remaining HVCs to exhibit lower-intensity $H\alpha$ emission than either set of detections because nearly all of them would be either farther away from the source of leakage radiation or in a much lower-density portion of the halo. Observations of a number of other HVCs show that the detections or upper limits are reasonably consistent with this picture. Weiner (1998) has observed 4 HVCs over a range of longitudes and has obtained upper limits of 60 mR toward all of them. Kutyrev & Reynolds (1989) detected $H\alpha$ toward an HVC in Cetus at a level of 81 mR, only 20% of the intensity of the weakest of the Weiner & Williams (1996) detections, and comparable to the weakest of the Tufte et al. (1998) detections. Thus, at least four of these five clouds appear to be farther than Complexes A, C, and M and the Magellanic Stream, regardless of the source of ionization.

Bland-Hawthorn & Maloney (1997) have modelled the ionizing photons leaking from the Galactic disk in order to derive an expression for the mean EM of an HI cloud as a function of distance from the Galactic plane. For their preferred value of the optical depth of the disk material to radiation at the Lyman limit, 2.8, which best fits the Weiner & Williams detections, they obtain $EM = 6.7 \times 10^2 r_{\text{kpc}}^{-2} \text{ cm}^{-6} \text{ pc}$; for $\tau = 2$, the coefficient rises to 1.8×10^3 . An EM of $6.7 \times 10^2 \text{ cm}^{-6} \text{ pc}$ corresponds to an intensity of about 270 R, three orders of magnitude greater than the Magellanic Stream detections. Even at a distance of 10 kpc from the plane, an EM of at least $7 \text{ cm}^{-6} \text{ pc}$ is expected, easily within the range of past and present observations. Bregman & Harrington (1986) also estimated the Lyman continuum flux leaking into the halo and obtain values similar to those of Bland-Hawthorne & Maloney. If these models are approximately correct, one would also expect that a Galactic HVC with a vertical distance of only a few kpc would be evident on optical photographs such as the POSS images, which have an emission measure sensitivity of $\sim 100 \text{ cm}^{-6} \text{ pc}$. Furthermore, given the detection of shock-excited $H\alpha$ in the Magellanic Stream, one would expect higher intensities from all of the HVCs with larger radial velocities and from most with lower velocities because of the much higher density of ambient gas in the lower Galactic halo if the HVCs are Galactic. Given the level of detections in the Magellanic Stream and in Complexes A, C, and M, essentially all HVCs located in the Milky Way halo should be easily detectable in deep $H\alpha$ surveys such as the WHAM survey (Reynolds 1996).

At large distances from the Milky Way and M31, HVCs should be detectable from the ionization expected from the diffuse ionizing background radiation, for which there is currently a $2\text{-}\sigma$ upper limit to the flux of 20 mR (Vogel et al. 1995). This ionizing flux would lead to an EM of $4 \times 10^{-2} \text{ cm}^{-6} \text{ pc}$. On the other hand, if the background ionization is as low as $6 \times 10^{-24} \text{ erg cm}^{-2} \text{ s}^{-1} \text{ Hz}^{-1}$, as suggested by Kulkarni & Fall (1993), the EM from extragalactic HVCs could be as low as $2 \times 10^{-3} \text{ cm}^{-6} \text{ pc}$; this would be the minimum EM expected from an HVC, Galactic or extragalactic. It is unclear at present whether the diffuse background flux or the ionizing flux leaking from the Milky Way and M31 dominates

the Lyman–limit flux absorbed by the HVCs.

7.2. HVC Metallicities

Metallicity determinations should provide one of the clearest tests of whether the HVCs are Galactic or extragalactic. If the HVCs are Galactic, then they would have abundances that are at least solar. In a Galactic–fountain model, for example, gas ejected from the inner Galaxy would have abundances greater than solar because the Galactic metallicity gradient implies high metallicity in the inner Galaxy. Gas that is simply ejected vertically and falls back vertically does not attain high velocities relative to the LSR. Furthermore, if the source of the fountain is gas ejected into the corona by massive stars and supernovae, this gas should be metal enriched, even at the solar circle.

In the Local–Group infall model, on the other hand, we expect that HVCs would have metallicities typical of the intergalactic medium. This characteristic metallicity is poorly known, but is probably significantly greater than the primordial abundance. In poor groups, X-ray observations imply metallicities ~ 0.1 solar (Davis et al. 1996). This non–primordial abundance likely represents the chemical pollution of the intergalactic gas. ASCA observations of rich clusters find metal abundances of roughly half the solar abundance (Mushotzky et al. 1996). Based upon the large metal abundances seen in intercluster gas, Renzini (1997) suggested that the metal abundance of the intergalactic medium has today reached 1/3 of the solar value. Thus, even though we identify the HVCs as gas clouds which are falling into the Local Group for the first time, their phenomenological association with Ly– α absorbers suggests that their metallicities would be subsolar, with values of ≤ 0.1 to 0.3 solar, but not primordial.

Abundance measurements from absorption–line studies show, on the other hand, that HVCs always have metallicities significantly less than solar, generally ≤ 0.1 solar (Savage et al. 1993; Lu, Savage, & Sembach 1994; Sembach et al. 1995; Sembach & Savage 1996; Lu et al. 1997; see WvW97 for a review). However, because some lines are saturated, and because observed lines may not always be the dominant ionization stage, it is not always possible to obtain reliable metallicities from the observations. Furthermore, abundances of some species may be depleted onto grains, further complicating metallicity determinations. However, analyses of the IRAS and COBE data bases (Wakker & Boulanger 1986; Schlegel, Finkbeiner, & Davis 1997) suggest that the dust abundances in the Northern Hemisphere Complex are at least three times lower than the locally determined value. Also, because the HVCs are observed primarily at high Galactic latitudes, if they were Galactic then the HVCs should be more like the warm diffuse clouds where the gas–phase depletions are

considerably smaller. Thus depletion onto dust grains would be minimal because there is little dust on which to deplete the gas, and because the HVCs would, in any event, correspond to interstellar clouds where the depletion is already relatively minimal. Alternatively, the IRAS non-detections of HVCs may result from dust temperatures lower than those typically found in the Galactic plane; in that case, heating by the interstellar radiation field implies distances of at least 10 kpc from the Galactic plane (Wakker & Boulanger 1986), a value consistent with the Local Group hypothesis.

One HVC was measured to have an S/H ratio of 0.25 solar (Lu et al. 1997), which should represent its true metallicity, because sulfur is not readily depleted onto grains and because the SII transition observed should be the dominant ionization stage of the ion. Lu et al. conclude that this metallicity suggests a Magellanic Cloud origin, even though the HVC in question is not part of the Magellanic Stream. The metallicity is reasonably consistent with the Local-Group hypothesis, but inconsistent with a Galactic origin. Complex C in the Northern Hemisphere grouping exhibits a MgII line with an abundance of 0.10 solar and another, higher-velocity component (associated with cloud 84 in the WvW91 catalogue and presumably not part of the Northern Hemisphere Cloud), with an abundance of 0.06 solar (Bowen & Blades 1993; Bowen et al. 1995; WvW97). Sembach & Savage (1996) give somewhat different abundances, an order of magnitude lower in the case of cloud 84, but always well below solar values. For MgII the ionization correction should not cause significant uncertainty, although Sembach & Savage point out that the results may be affected by dust depletion. The expected depletion for magnesium in warm halo gas is, however, only about a factor of three on average (Sembach & Savage 1996); these two clouds may be reasonably considered to be metal deficient even for halo gas, contrary to expectations if the gas originated in a Galactic fountain. We therefore find that of two lines of sight with three individual HVCs, there are metal deficiencies of as much as a factor of twenty, and that no line of sight has abundances that even approach solar values.

7.3. Extragalactic HVC Searches

If HVCs are indeed characteristically extragalactic, and are the leftover building blocks from which the Local Group formed, similar entities would be expected to be observed toward other galaxy groups. Because the details of the distribution would depend on the dynamics of the particular galaxy group being observed, the detailed spatial and kinematic patterns of the Local Group would not be preserved. The general properties of the HVC phenomenon would, however, be preserved out to the Hubble-flow turnaround radius of the galaxy group in question, and might be observable with radio interferometers or, in some nearby groups,

with single dishes. As we discuss below, such clouds have apparently been detected.

We first consider the sensitivity of the VLA and of single dishes for a search for extragalactic HVCs. For the VLA, the brightness sensitivity is greatest in the most compact configuration, the D-Array; maximum sensitivity is attained when the velocity channels are the broadest. If we assume that the channels are 20 km s^{-1} wide, equal to the mean linewidths of the HVCs in Table 1, and that all 27 antennas are used for an integration time of 8 hours (a single earth-rotation synthesis), we obtain an rms brightness sensitivity of 0.12 K. A detection with this many pixels and a single velocity channel requires a minimum signal-to-noise ratio of 5σ , or an equivalent mean column density of $2.2 \times 10^{19} \text{ cm}^{-2}$ in a synthesized beam with a diameter of $44''$. This estimate is a lower limit to the detectable column density because it assumes observing at the zenith, 100% system efficiency, and natural weighting.

We now further assume that we are trying to detect an HVC system identical to the one we associate with the Local Group, with a turnaround radius of 1.5 Mpc and a mean HVC diameter of 28 kpc. The primary beam (i.e. field of view) is $30'$; a cluster of Local-Group HVCs would have to be at a distance of 340 Mpc to fill this primary beam. The synthesized beam (resolution element) at this distance is 73 kpc, diluting the signal by a factor of 6.7 and raising the minimum detectable column density by the same factor. Thus, one would detect HVCs with a mean $N_{\text{HI}} > 1.5 \times 10^{20} \text{ cm}^{-2}$; Figure 16 shows that there are only two Galactic HVCs with such large column densities. The detection threshold would increase if the clouds just fill the synthesized beam, which would occur for a system at a distance of 130 Mpc, but, at that distance, one would decrease the total number of clouds in the primary beam by a factor of 6.7. Given the frequency distribution of column densities shown in Figure 16, we find that only 5.5% of the HVCs have $N_{\text{HI}} > 2 \times 10^{19} \text{ cm}^{-2}$, and only 2.0% have $N_{\text{HI}} > 3 \times 10^{19} \text{ cm}^{-2}$, a more realistic detection limit. If another system at a distance of 130 Mpc has the same number of clouds as the Local Group, some 550, one would expect to detect only 5 clouds at a threshold column density of $2 \times 10^{19} \text{ cm}^{-2}$, and only 2 clouds at a threshold of $3 \times 10^{19} \text{ cm}^{-2}$.

All extragalactic searches have, however, focused on galaxies with distances less than 130 Mpc. In such nearby searches, the significance of a detection in a single pixel is not substantially increased unless a large fraction of the surface area of an HVC is at a column density much above the mean. In that case, one might be able to detect the higher-column-density parts of an HVC with lower sensitivity observations, yielding a size smaller than that of the cloud as a whole. Spatial averaging could also increase the significance of a detection. On the other hand, the smaller area covered by the primary beam means that there is a decreasing probability of intersecting a single cloud ($\propto d^{-2}$), such that the probability of

detecting a cloud in a cluster at a distance of 13 Mpc, for example, is 0.05 at a column density of $2 \times 10^{19} \text{ cm}^{-2}$, if the clouds are uniformly distributed within the turnaround radius. The detection probability increases with the square of the distance and is further increased if the distribution of HVCs is not random but shows some concentration in the deeper parts of the potential well, close to the most massive galaxies in the cluster. In that case, a good strategy would involve targeted searches near massive galaxies in poor groups. The detection probability is also enhanced to the degree that the WvW91 compilation is incomplete. For most searches to date, we estimate that the probability of a detection with a radio interferometer of a single HVC like those in the Local Group is generally less than unity, but probably more than ~ 0.1 , depending on the galaxy–cluster environment and its distance, suggesting that some extragalactic HVCs might already have been detected. In any event, we expect that interferometric searches would rarely detect more than one cloud in the primary beam for nearby objects, and no more than a few clouds at large distances.

For single–dish searches, the brightness sensitivity is much greater than with an interferometer, but at distances greater than 3 Mpc an HVC would be unresolved with a 25–m dish. A 5σ detection of a cloud with a mean column density of $1 \times 10^{18} \text{ cm}^{-2}$ at 3 Mpc requires about 1/2 hour of on–source integration time with a sensitive system, or a total of about 1 hour in real time. Such an observation would detect any cloud in the WvW91 compilation. However, the surface filling fraction of those clouds is only 5%; about 20 hours of observing would be necessary to find one cloud at a distance of 3 Mpc. Most small groups of galaxies lie at greater distances, and although the probability of intersecting a cloud goes up as the square of the distance, the signal from a single cloud is decreased by the same factor, and one detects only the higher–column–density HVCs for a fixed integration time. As with interferometers, the detection probability depends on the unknown degree of clustering of the HVCs, and on the incompleteness of the WvW91 compilation. With a small (25–m to 50–m) antenna, one expects that a detection would be manifested as an asymmetric wing on an HI line profile. Bates & Maddalena (1996) searched for high–velocity wings using the NRAO 43–m telescope and found such wings toward 8 of the 23 galaxies observed. Further analysis and interferometric observations are required to determine whether this gas is like the Local–Group HVC ensemble, but their observations suggest that single dishes might be able to detect extragalactic HVC candidates. The newly–upgraded 300–m Arecibo telescope affords approximately the same column–density sensitivity as smaller dishes, but has a much smaller beam which would resolve HVCs out to distances of about 30 Mpc. However, one still expects only a few detections in 20 hours of observation because of the expected small surface–filling fraction of the HVCs. We therefore conclude that detection of HVC analogues in other systems should be possible with a good search strategy and a sufficient investment of observing time.

Several published HI searches have turned up clouds which resemble what we expect for extragalactic HVCs. Observations by van der Hulst & Sancisi (1988) toward the giant Sc galaxy M101 showed two clouds superimposed on the disk with radial–velocity differences of 130 and 160 km s^{−1} from normal galactic rotation. The masses of those clouds are 1.6×10^8 and $1.2 \times 10^7 M_\odot$ and the diameters are 16 kpc and 5 kpc, respectively, for $H_0 = 75 \text{ km s}^{-1} \text{ Mpc}^{-1}$. Van der Hulst & Sancisi argued that the M101 HVCs must be completely different from even the largest and most massive of the Milky Way HVCs, if the latter are objects in the Galactic halo at distances less than 10 kpc. The very large kinetic energy ($\sim 10^{55}$ erg) of the M101 clouds relative to the host galaxy implies that they are being accreted by the galaxy rather than being expelled. The mass and diameter of the larger M101 cloud is comparable to the mean value given in Table 3 for the Local Group HVCs, and is thus consistent with its being an HVC similar to those inferred in this paper. Furthermore, the similarity in the velocities of the two clouds discovered by van de Hulst & Sancisi suggest that they might be fragments of a single object falling onto M101.

Kamphuis & Briggs (1992) found two HVCs toward the galaxy NGC 628 with masses of $7.9 \times 10^7 M_\odot$ and $9.5 \times 10^7 M_\odot$ (for $H_0 = 75 \text{ km s}^{-1} \text{ Mpc}^{-1}$) in the outer parts of the NGC 628 disk which they, too, attribute to accretion. The mean diameters of these clouds are 38 kpc and 47 kpc, respectively; the respective peak HI column densities are 1×10^{20} and $3.7 \times 10^{19} \text{ cm}^{-2}$, values within the range of what is observed for the Local–Group HVCs. A third, smaller HVC is argued to be possibly related to one of the larger clouds.

More recently, Schulman et al. (1996) detected and mapped an extragalactic HVC toward NGC 5668 with the VLA. Using a simple rotational model for the HI in NGC 5668, the authors identified HI emission that is kinematically distinct from the galaxy itself and found a cloud beyond the optical disk of the galaxy, extending in fact even beyond the outer edge of the HI disk. Although the cloud blends with the emission from the disk of the galaxy, the diameter of the cloud is estimated to be about $4'$. Schulman et al. conclude that this feature is distinct from the HI in the disk and cannot be due to a galactic fountain. At a distance of 21 Mpc (for $H_0 = 75 \text{ km s}^{-1} \text{ Mpc}^{-1}$), the cloud has a diameter of about 25 kpc, and an HI mass of $1 \times 10^8 M_\odot$. The mass follows from the total amount of kinematically distinct gas determined by Schulman et al. and adjusted for their different value of H_0 .

HVC analogues have also been found by Taylor et al. (1995), who made a VLA search for companion objects to HII galaxies. They found six HI clouds without optical counterparts, in the fields of 21 galaxies. These intergalactic HI clouds have masses in the range 0.6 to $1.7 \times 10^8 M_\odot$, and diameters ranging from 8 to 16 kpc. Further, Hunter, van Woerden, & Gallagher (1994) found a cloud with a mass of $6 \times 10^7 M_\odot$ and a diameter of ~ 7 kpc toward NGC 1800.

Clearly, numerous extragalactic HI clouds have already been found, with properties similar to those we infer for the HVCs associated with the Local Group. Several of these (in particular those of Taylor et al. 1995) show no direct spatial or kinematic connection with the target galaxy. The others may be extragalactic analogs of Complex C, which we argued above is probably being tidally disrupted as it is being accreted by the Milky Way. We predict that observations in fields adjacent to other massive galaxies will also turn up HI clouds with properties similar to those given in Table 3, at about the rate determined by the detectability criteria above.

7.4. Re-examining Arguments Against the Extragalactic Origin of HVCs

Several cogent arguments have been offered against the extragalactic origin of HVCs (see WvW97 and references there, especially Giovanelli 1977 and 1981, and Verschuur 1975). These arguments include the following: (1) the kinematics of galaxies in the Local Group do not match the HVC kinematics; (2) if the HVCs are bound, then either they extend beyond the Local Group or else some 90% of their mass is in a form other than neutral hydrogen; (3) no explanation is available for the multi-phase nature of the HVCs, in particular, for the cold gas seen in the HVC cores; (4) the small velocity gradients seen in the clouds remain enigmatic; and (5) analogous systems of clouds are not detected near external galaxies. These criticisms were made when the observational situation was much less mature than it is now. Specifically, the sky north of $\delta = -30^\circ$ is now quite uniformly surveyed in the HI line, over the velocity range which encompasses the HVC phenomenon. There is observational evidence for anomalous-velocity structures in the vicinity of external galaxies, and the astrophysical context now encompasses the idea of galaxy growth through accretion of relatively modest clouds which may contribute dark and ionized matter as well as the observed neutral gas.

It seems that the earlier arguments against the extragalactic HVC origin do not pertain for the Local Group infall hypothesis which we have discussed here.

- We showed in §5 and §6 that the kinematics of infalling gas does, in fact, match the observed HVC kinematics.

- We indicated in §4 that there is roughly 10 times more dark matter than luminous gas associated with each HVC, the same ratio of dark matter to matter accounted for as in galaxies and on cosmological scales.

- We argued in §6 that gas in dark matter halos with velocity dispersions of 10 to 30 km s^{-1} will form a two-phase structure as the denser gas in the dark-matter cores cools and is shielded from the intergalactic ionization field.

- We showed in §6 that the small velocity gradients occur because the HVCs are gravitationally focused into large-scale filaments.

- We pointed out in §6 that quasar absorption-line studies do, in fact, reveal clouds with HI column densities of 10^{18} to 10^{19} cm^{-2} , namely the Lyman-limit systems associated with galaxy groups, and in §7 that HI analogues have been detected toward a number of other galaxies through 21-cm aperture synthesis.

8. Implications for the Evolution of the Milky Way

8.1. Infall Rates and Implications for Star Formation

If the Milky Way and M31 are accreting material in the form of HVCs, it is possible to estimate the infall rate from the simulation discussed in §6.2, normalized by the total HVC mass currently observed. The results of this estimate are shown in Figure 17. The accretion rate is determined by assuming that any cloud in the simulation that passes within 100 co-moving kpc of the center of either the Milky Way or M31 is ultimately absorbed by that galaxy. This is a gross simplification of the accretion process, but it is nonetheless useful to explore the accretion history in the simulation.

The upper panel of Figure 17 shows that accretion is rapid early on, reaching a peak at about 30 times the current rate for the Milky Way within a billion years after the beginning of the simulation. Although the accretion rate for M31 is about twice that of the Milky Way in the first few billion years, the rates at the present epoch are nearly equal. About half of the mass accreted by the Milky Way falls onto it during the first 2 billion years. Using the direct normalization from the simulation, the present-day accretion rate shown in Figure 17 for the Milky Way is $7.5 M_{\odot} \text{y}^{-1}$, corresponding to a neutral-gas accretion rate of about $1.2 M_{\odot} \text{y}^{-1}$.

Another way to estimate the accretion rate is by comparison with the observed HVCs. Figure 17 shows that roughly 30% of the total mass accreted by the Milky Way has been acquired during the past 9 billion years. As mentioned in §6, this mass is approximately equal to the mass currently observed in HVCs, and is about 25% of the original inventory. There are 518 HVCs in the WvW91 compilation that are not part of the Magellanic Stream. Comparison of the compilation with maps made from the LD survey revealed a number of small clouds not in the WvW91 catalogue because they lie between the grid points of the coarser surveys; the incompleteness, however, probably changes the total number by less than a factor of two. Thus the total mass in HVCs at the present time is contributed by ~ 1000 clouds with a mean mass of $3 \times 10^8 M_{\odot}$, or $3 \times 10^{11} M_{\odot}$. Roughly 50% of the

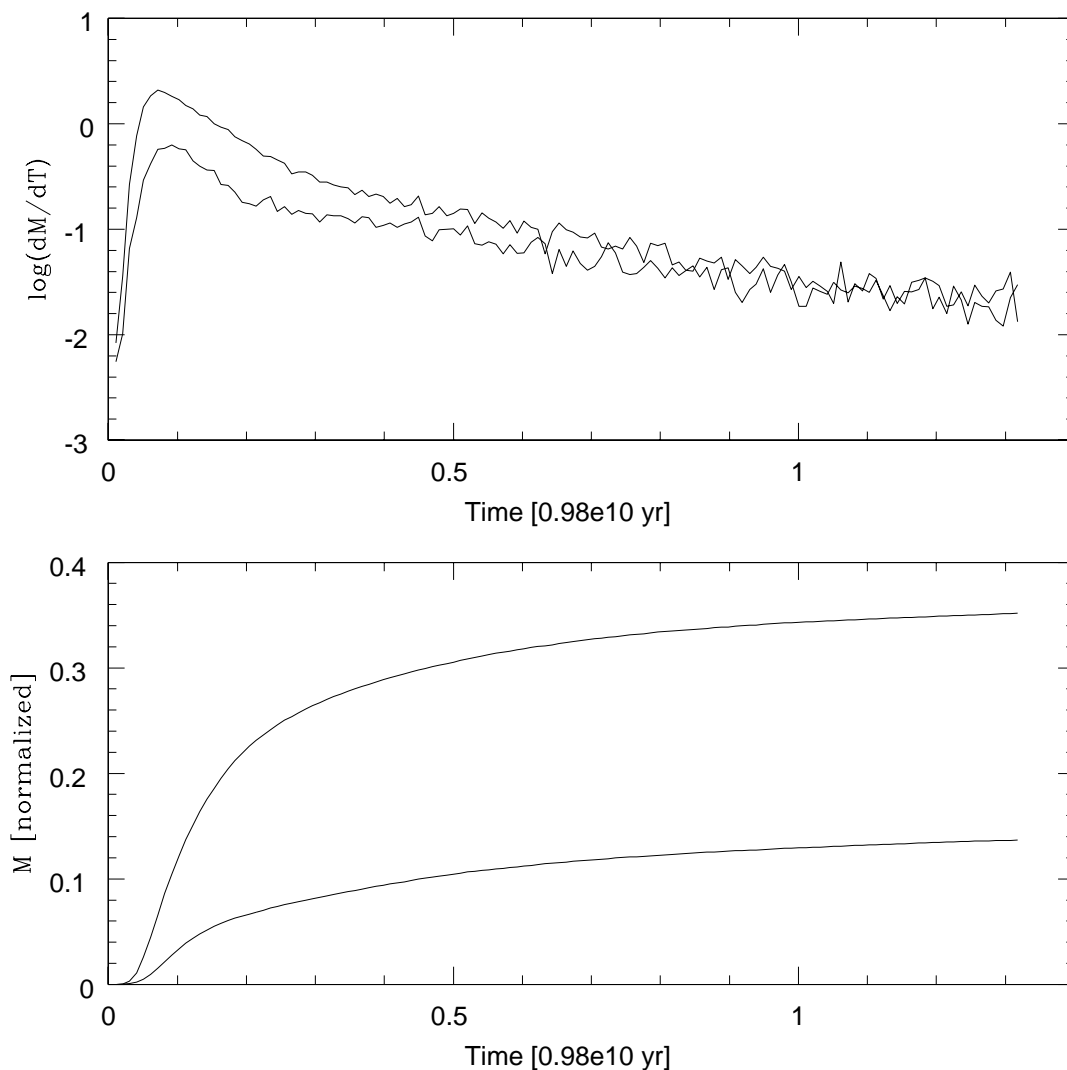


Fig. 17.— *Upper:* Normalized rate of simulated accretion of clouds for the Milky Way (lower line) and for M31. The M31 accretion rate is typically about twice that of the Milky Way. After about 3 billion years the accretion rate becomes nearly exponential with an e-folding time of about 5×10^9 y. At the current epoch, the accretion rate is flattening out, and is equivalent to about $7.5 M_{\odot} \text{ y}^{-1}$ for the Milky Way. *Lower:* Normalized accreted mass for the Milky Way (lower line) and M31. The plot shows that most of the mass is accreted at early times and that additional mass is being added to both galaxies quite slowly at the current epoch.

total accreted over the past 12 billion years corresponds to an average rate of $12.5 M_{\odot} \text{ y}^{-1}$. Figure 17 indicates that there have been about 2 e-folding times in the past 12 billion years. The present-day total accretion rate should be about $1/e$ of the average rate of about $4.6 M_{\odot} \text{ y}^{-1}$, or a neutral-gas accretion rate of $\sim 0.8 M_{\odot} \text{ y}^{-1}$, in reasonable agreement with the accretion rate given above.

We should not take these numbers as more than rough estimates, in view of the uncertainties and simplifications present in the simulation. The gas accretion rate, for example, would be significantly larger if a large quantity of ionized gas were associated with the HVCs. It is worth noting in this context that Lacey & Fall (1985) and Blitz (1997) have argued that the short (2 to 5×10^8 y) molecular-gas depletion time for the Milky Way could be compensated with gas infall equal to the net rate of gas conversion into stars, some 1 to $3 M_{\odot} \text{ y}^{-1}$. The gas accretion rate we infer for the HVCs is within this range, and could provide the fuel for the continuing star formation in the Milky Way and in spiral galaxies in general.

8.2. The Galactic Fountain

The most frequently discussed origin for the HVC phenomenon is the “galactic fountain” proposed by Shapiro & Field (1976) and elaborated by Bregman (1980) and others. In the galactic-fountain model, gas is heated by supernova explosions in the disk to temperatures of $\sim 10^6$ K, convects to the Galactic corona where it radiatively cools, and then falls back to the disk as high-velocity gas. To explain the high velocities observed at latitudes away from the zenith, Bregman requires a radial outflow which conserves angular momentum; this outflow cannot account for radial velocities larger than about $\pm 200 \text{ km s}^{-1}$, yet many HVCs are observed with higher velocities. The galactic-fountain model makes several other predictions about the nature of the HVCs (see Wakker & Bregman 1990): the HVCs would be metal rich because the gas is largely ejected from the inner Galaxy ($Z > Z_{\odot}$); their characteristic distances would be between 0 and 10 kpc from the Galactic plane; and their vertical velocities would be less than 70 to 100 km s^{-1} .

The predictions of the galactic fountain model are not consistent with many of the observations of the ensemble of HVCs. The HVCs observed to date all have substantially subsolar abundances and at least two have subsolar metallicities (see §7.2). If the heavy elements in the clouds were bound into dust grains in clouds at distances less than 10 kpc, then the HVCs would have been detected in the IRAS $60 \mu\text{m}$ band, but they were not detected (Wakker & Boulanger 1986). Absorption-line observations towards AGNs imply that the filling fraction for HVCs at column densities as low as $1 \times 10^{17} \text{ cm}^{-2}$ is a factor

of 1.5 to 2.0 greater than that found in emission in WvW91 (Murphy et al. 1995; Bowen et al. 1995). Excluding the Magellanic Stream and the Outer Arm Complex, this implies a surface filling fraction of 20% down to these low column densities, yet only two lines of sight have yielded positive absorption–line detections of the dozens (or more) stars towards which high–velocity absorption has been sought. This result is difficult to understand if the characteristic distance to an HVC is only a few kpc. Finally, many HVCs have vertical velocities that exceed 100 km s^{-1} .

One of the attractions of the galactic fountain model is that it seems naturally to fit into a coherent picture for the dynamics of the interstellar medium. Supernovae eject significant amounts of mass into the ISM and drive gas upwards through chimneys (Heiles 1990). McKee (1993) estimates an outflow rate of several solar mass per year. Mass balance seems to require that this gas is somehow returned to the disk.

Is there evidence for the existence of a Galactic fountain? We carried out a decomposition of the individual spectra of the LD survey into velocity components, identified from intensity maxima in each spectrum, and selected according to a minimum velocity width. This selection tends to bias the resulting component list against high–velocity emission. Figure 18 summarizes the results of the decomposition and was produced by marking with a dot each velocity component in the list at a given Galactic latitude, independent of its longitude. The plot is therefore a latitude–velocity plot of HI velocities which accentuates the emission observed at low velocities. The dominant feature in Figure 18 is the nearly vertical band of emission, but note that the emission near 0 km s^{-1} toward both Galactic poles is negative, smoothly increasing to slightly positive values near the Galactic equator. Gas near 0 km s^{-1} is overwhelmingly local, but in a static HI layer, the velocities would be precisely zero at latitudes away from the Galactic equator. (At $|b| \sim 0^\circ$, the Galactic rotation along the long lines of sight intercepted would introduce some non–zero velocities, slightly positive when averaged over the longitude range of the LD survey.). An error in the determination of the LSR would have a different signature, resulting in deviations of equal magnitude but opposite signs in the two Galactic hemispheres. Rather, Figure 18 suggests that the gas is falling toward the plane in both hemispheres. The predominance of negative velocities toward the poles has been known for many years (see e.g. Weaver 1974; Kulkarni & Fich 1985; Lockman & Gehman 1991). We note that the deviation from zero velocity is quite symmetric with respect to the Galactic plane, implying that the gas motions are both systematic and quite general.

If the motions implied by Figure 18 represent vertical infall onto the Galactic plane, then the velocities should show a $\sin b$ dependence which other systematic motions would not show. Figure 19 shows the mean of the velocity components, averaged over all longitudes at each

Fig. 18.— Latitude-velocity plots of all of the individual velocity components in the LD survey biased by velocity width to deemphasize high-velocity emission. Each component from each spectrum is plotted as a dot in the figure.

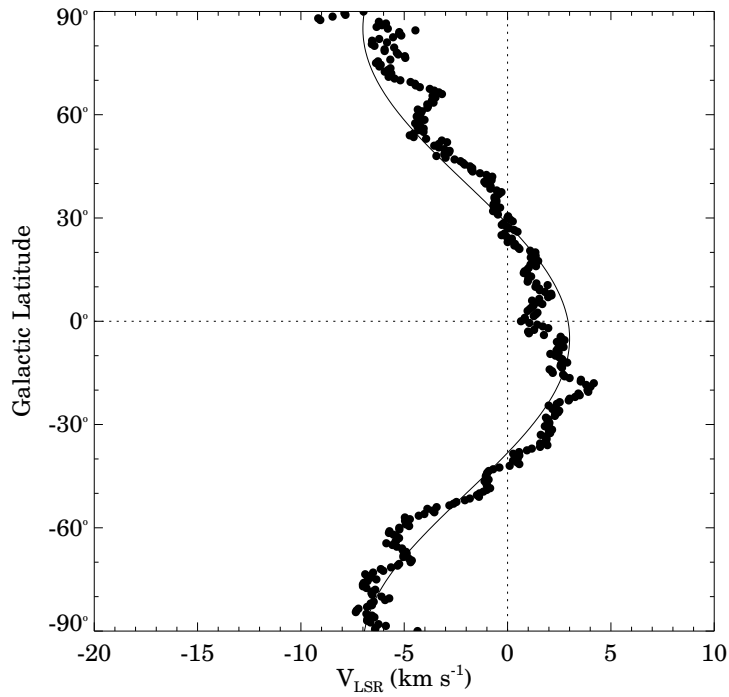


Fig. 19.— Components from Figure 18 averaged over longitude at each 0.5 of latitude (the resolution of the LD survey) for $|v_{l,ST}| < 20 \text{ km s}^{-1}$. What is plotted is therefore represents all of the local HI (out to 500 – 1000 pc) within the disk. A disk in hydrostatic equilibrium would show all velocities at 0 km s^{-1} . See text for the equation of the fitted sine curve.

latitude of the LD survey, for the local gas, which is obtained by restricting the calculation of the mean to an LSR velocity range within $\pm 20 \text{ km s}^{-1}$ of zero. Superimposed on the data is the least-squares fit $v_{\text{LSR}} = -1.8 - 4.5 \sin(2b - 49) \text{ km s}^{-1}$. Deviations from the fit are generally less than 1 km s^{-1} , showing that a sine curve is a good description of the data; such a functional form implies vertical infall. The LD survey is not an all-sky survey, however, so we checked the eventual effect of the incomplete sky coverage on the Figure 19 curve by making latitude-velocity plots separately in different longitude ranges. Although the LD coverage in the first quadrant is complete in both longitude and latitude, and quite incomplete in the third and fourth quadrants, the general shape and magnitude of the curve shown in Figure 19 is present in all quadrants, implying that the motion seen in the figure is a general property of the local gas. The results imply that the entire HI layer is collapsing toward the equator at a velocity of 6.3 km s^{-1} , out to a distance of at least several hundred pc, i.e. the radial distance probed at $b = 30^\circ$. This is an average gas motion; although there may be local deviations, the local HI layer is apparently not in hydrostatic equilibrium.

We propose that the inflow toward the plane of the HI layer is a manifestation of the Galactic fountain; but rather than velocities of tens up to 100 km s^{-1} , the returning flow evidently does not exceed the sound speed of the material in which it is embedded. Thus the returning gas, once it has become neutral, does not have a vertical velocity in excess of about 10 km s^{-1} . The infall velocity is regulated by mass conservation at different heights above the plane and by the requirement that the gas motions not be supersonic, at any z -height. Furthermore, the data suggest that the motions are almost entirely in z , as suggested originally by Shapiro & Field (1976), without a large radial component.

We estimate the mass infall rate, dM/dt , from $dM/dt = \rho Av$, where ρ is the mean density of the neutral gas, v its mean infall velocity, and A the area of the Milky Way onto which the gas falls. N_{HI} is well determined toward the Galactic poles and has an average value of $1.7 \times 10^{20} \text{ cm}^{-2}$ (Kulkarni & Fich 1985). We take ρ as $N_{\text{HI}} m_{\text{HI}} / z_{\text{HI}}$, where z_{HI} is the total thickness (i.e. twice the scale height) of the HI layer, a loosely defined concept unless the emission is deconvolved into separate components (see e.g. Falgarone & Lequeux 1973; Lockman & Gehman 1991). If we take z_{HI} to be twice the scale height in units of 1 kpc, and if we assume that what we observe locally is representative of the infall out to a distance of 10 kpc from the Galactic center, then, correcting for helium, $dM/dt = 5.3 z_{\text{HI}} M_{\odot} \text{ y}^{-1}$. If most of the HI seen toward the galactic poles is the cold HI component, then $z_{\text{HI}} = 400 \text{ pc}$ (Falgarone & Lequeux 1973; Lockman & Gehman 1991), and $dM/dt = 2.1 M_{\odot} \text{ y}^{-1}$. If the Galactic fountain returns gas to radii as large as 15 kpc, or about twice the Sun’s distance from the center, dM/dt increases by a factor of 2.3. Thus for the expected range of HI scale height and radius over which the Galactic fountain operates, the expected infall rate from Figure 19 is several $M_{\odot} \text{ y}^{-1}$. However, unlike the detailed fountain models proposed to date,

the observations imply that the return flows are subsonic and almost entirely normal to the plane.

We now compare the measured mass infall rate with the estimated mass injection rate into the Galactic halo by supernovae. Taking all of the phases of HI into account, and extrapolating to a radius of 10 kpc, (Heiles (1990) obtained a mass injection rate of $1.7 M_{\odot} \text{ y}^{-1}$, in agreement with our estimated infall rate of $2.1 M_{\odot} \text{ y}^{-1}$. McKee (1993) found a similar mass injection rate of several $M_{\odot} \text{ y}^{-1}$. Thus even though the HI layer is evidently not in hydrostatic equilibrium, the total gas layer in the disk and corona appear to be in steady-state dynamical equilibrium.

8.3. Chemical Evolution of the Disk

The above analysis has implications for understanding the evolution of the Galactic disk. The constant rain of high-velocity clouds implies that the disk experiences episodic accretion of gas. The relatively weak Galactic fountain discussed above implies slow radial mixing of metals. The combination of these two effects would lead to a chemically inhomogeneous interstellar medium, with large radial metallicity gradients.

There is, in fact, evidence for significant chemical inhomogeneities in the Galactic disk. Edvardsson et al. (1993) carried out a high-resolution study of disk stars, finding both a remarkably small scatter in $[\alpha/\text{Fe}]$ at fixed age and Galactic distance, and a relatively large scatter in $[\text{Fe}/\text{H}]$ at fixed age. Their study also confirmed the classic G-dwarf problem. They suggest that these trends reflect the combination of episodic accretion and relatively inefficient mixing. Friel & Janes (1993) found a large spread in metallicity at fixed age, also consistent with the combination of episodic accretion and slow mixing. The chemical-evolution models of Pilyugin & Edmunds (1996) confirm that this combination accounts for the observed metallicity trends.

Observations of chemical abundances in Orion also appear to confirm the combination of episodic accretion plus local enrichment scenario. Meyer et al. (1994) argue that the low oxygen abundance in Orion, some 40% of the solar value, suggests recent infall. The Cunha & Lambert (1992, 1994) studies of OB associations found evidence for local self-enrichment of this gas.

9. Conclusions and Predictions

Most cosmologists believe that galaxy formation is a hierarchical process: galaxies grow by accreting small clouds of gas and dark matter. This process is a continuing one and we expect that galaxies and groups are currently accreting new clouds. We simulated this process for the Local Group and found that properties of the accreted clouds are similar to certain properties of the high-velocity-cloud phenomenon (excluding the Magellanic Stream HVCs):

- Most of the HVCs are located either near the general direction of M31, towards the barycenter of the Local Group, or in the antibarycenter direction, some 180° from the direction of M31 (see Figure 14).

- HVCs have chemical abundances similar to that of intra-group gas, and different from the abundances characteristic of the inner Galaxy. If HVCs were ejected from the inner Galaxy as part of a Galactic fountain, then their metal abundance would exceed the solar value, and this is not observed.

- HVCs have an angular-size/velocity relation that is consistent with the clouds being nearly self-gravitating, and at a distance of ~ 300 kpc.

If the Local-Group HVC hypothesis discussed in this paper is correct, then studies of HVCs can directly probe the process of galaxy formation. The validity of this hypothesis can be tested by a number of future observations:

- Most observations of nearby galaxies would not have detected the gas clouds that are equivalent to the HVCs. Moreover, many HI maps of external galaxies extend just beyond the Holmberg radius. Our discussion would have the typical HVC located nearly a Mpc from the galactic center. It will be interesting to test our hypothesis with deep HI observations of isolated groups and filaments, searching for HI clouds associated with groups, rather than with individual galaxies.

- Lyman-limit clouds, which are seen in absorption towards distant quasars, have column densities similar to those of the HVCs. Observations of nearby Lyman-limit and Lyman- α systems show that they are not all associated directly with individual galaxies, but rather with groups of galaxies (Oort 1981; Stocke et al. 1995; van Gorkom et al. 1996; Rauch, Weymann, & Morris 1996). In the scenario outlined in this paper, we expect that these clouds would have properties similar to those of the local HVCs. Thus, it would be interesting to use STIS to look for lower-column-density high-velocity HI clouds, which would correspond to the Lyman- α clouds.

- The simulations predict large amounts of gas accreting onto M31 and the Local Group

from the region of space beyond M31, under the gravitational attraction of both M31 and our own Galaxy. Because this gas is several Mpc away, the gas clouds are expected to have small angular sizes and relatively low column densities. Deep HI observations in the M31 direction should be able to detect this gas.

The hypothesis central to this paper, namely that HVCs are at distances of around 1 Mpc, would be falsified by the detection of absorption in an HVC seen against stars in the Milky Way halo in the direction of M31 or in the anti-M31 direction. On the other hand, further measurements of low levels of $H\alpha$ emission towards these HVCs will strengthen the case for their extragalactic nature.

10. Acknowledgements

We have had useful conversations with many people about this work in the last year and a half; it is difficult to do justice to all of them. We are particularly grateful to Bart Wakker for providing a machine readable version of the WvW91 compilation, and for many discussions via the Internet. We are grateful for the comments and insights provided by George Field, Jacqueline van Gorkom, Dave Hollenbach, Buell Jannuzi, Jay Lockman, Dan McCammon, Chris McKee, Blair Savage, and Amiel Sternberg.

REFERENCES

- Arp, H. 1985, *AJ*, 90, 1012.
- Arp, H., & Sulentic, J.W. 1991, *Ap&SS*, 185, 249
- Babul, A., & Rees, M.J. 1992, *MNRAS*, 255, 346
- Bajaja, E., Cappa de Nicolau, C.E., Cersosimo, J.C., Loiseau, N., Martin, M.C., et al. 1985, *ApJS*, 58, 143
- Bajaja, E., Morras, R., & Pöppel, W.G.L. 1987, *Pub. Astr. Inst. Czech. Ac. Sci.*, 69, 237
- Bates, N., & Maddalena, R.J. 1996, *BAAS*, 28, 839
- Bi, H., & Davidsen, A.F. 1997, *ApJ*, 479, 523
- Bland-Hawthorn, J., & Maloney, P.R. 1997, *PASA*, 14, 59
- Blitz, L. 1997, in *CO: Twenty-Five Years of Millimeter–Wave Spectroscopy*, eds. W.B. Latter et al. (Dordrecht: Kluwer Acad. Pub.), 11
- Bond, J.R., Kofman, L., & Pogosyan, D. 1995, astro-ph/9512141
- Bond, J.R., Szalay, A.S., & Silk, J. 1988, *ApJ*, 324, 627
- Bond, J.R., & Wadsley, J.W. 1997, in *Computational Astrophysics, Proc. 12th Kingston Conference, Halifax, Oct. 1996*, eds. D. Clarke & M. West, astro-ph/9703125
- Bowen, D., & Blades, J.C. 1993, *ApJ*, 403, L55
- Bowen, D., Blades, J.C., & Pettini, M. 1995, *ApJ*, 448, 662
- Bregman, J.N. 1980, *ApJ*, 236, 577
- Bregman, J.N., & Harrington, J.P. 1986, *ApJ*, 309, 833
- Burton, W.B. 1997, in *The Physics of the Galactic Halo*, eds. H. Lesch, R.-J., Dettmann, U. Mebold, & R. Schlickeiser (Berlin: Akademie Verlag), 15
- Cen, R., Kang, H., Ostriker, J.P., & Ryu, D. 1995, *ApJ*, 451, 436
- Cen, R., Miralda-Escude, J., Ostriker, J.P., & Rauch, M. 1994, *ApJ*, 437, L9
- Cram, T.R., & Giovanelli, R. 1976, *A&A*, 48, 39
- Cunha, K., & Lambert, D.L. 1992, *ApJ*, 399, 586
- Cunha, K., & Lambert, D.L. 1994, *ApJ*, 426, 170
- Danly, L., Albert, C.E., & Kuntz, K.D. 1993, *ApJ*, 416, L29
- Davies, R.D. 1975, *MNRAS*, 1970, 45P
- Davis, D.S., Mulchaey, J.S., Mushotzky, R.F., & Burstein, D. 1996, *ApJ*, 460, 601

- Edvardsson, B., Anderson, J., Gustafsson, B., Lambert, D.L., Nissen, P.E., & Tomkin, J. 1993, *A&A*, 275, 101
- Einasto, J., & Lynden-Bell, D. 1982, *MNRAS* 199, 67
- Falgarone, E., & Lequeux, J. 1973, *A&A*, 25, 253
- Friel, E.D., & Janes, K.A. 1993, *A&A*, 267, 75
- Fukugita, M., Hogan, C.J., & Peebles, P.J.E. 1997, astro-ph/9712020
- Giovanelli, R. 1977, *A&A*, 55, 395
- Giovanelli, R. 1979, ???
- Giovanelli, R. 1981 *AJ*, 86, 1468
- Giovanelli, R., & Haynes, M.P. 1977, *A&A*, 54, 909
- Giovanelli, R., Verschuur, G.L., & Cram, T.R. 1973, *A&AS*, 12, 209
- Harris, W.E. 1996, *AJ*, 112, 1487
- Hartmann, D. 1994, Ph.D. Thesis, University of Leiden
- Hartmann, D., Kalberla, P.M.W., Burton, W.B., & Mebold, U. 1996, *A&AS*, 119, 115
- Hartmann, D., & Burton, W.B. (LD), 1997, *Atlas of Galactic Neutral Hydrogen*, (Cambridge: Cambridge Univ. Press)
- Heiles, C. 1990, *ApJ*, 354, 483
- Hernquist, L., Katz, N., Weinberg, D., & Miralda-Escude, J. 1996, *ApJ*, 457, L51
- Hoffman, G.L., Lu, N.Y., Salpeter, E.E., Connell, B.M., & Fromhold-Treu, R. 1998, astro-ph/9801189
- Hulsbosch, A.N.M. 1975, *A&A*, 40, 1
- Hulsbosch, A.N.M., & Wakker, B.P. 1988, *A&AS*, 75, 191
- Hunter, D., van Woerden, H., & Gallagher, J.S. 1994, *ApJS*, 91, 79
- Ikeuchi, S. 1986, *Ap&SS*, 118, 509
- Kahn, F.D., & Woltjer, L. 1959, *ApJ*, 130, 705
- Kamphuis, J., & Briggs, F. 1992, *A&A*, 253, 335
- Katz, N., Weinberg, D.H., Hernquist, L., & Miralda-Escude, J. 1996, *ApJ*, 457, L57
- Kepner, J., Babul, A., & Spergel, D.N. 1997, *ApJ*, 487, 61
- Kerr, F.J., & Sullivan, W.T. III 1969, *ApJ*, 158, 115
- Kulkarni, S.R., & Fall, S.M. 1993, *ApJ*, 413, L63

- Kulkarni, S.R., & Fich, M. 1985, ApJ, 289, 792
- Kutyrev, A.S., & Reynolds, R.J. 1989, ApJ, 344, L9
- Lacey, C.G., & Fall, S.M. 1985, ApJ, 290, 154
- Lada, C.J. 1985, ARA&A, 23, 267
- Lockman, F.J., & Gehman, C.S. 1991, ApJ, 382, 182
- Lu, L., Savage, B.D., & Sembach, K.R. 1994, ApJ, 426, 563
- Lu, L., Savage, B.D., Sembach, K.R., Wakker, B.P., Sargent, W.L.W., & Oosterloo, T.A. 1997, ApJ, submitted
- Mathewson, D.S., Cleary, M.N., & Murray, J.D. 1974, ApJ, 190, 291
- McGill, C. 1990, MNRAS, 349, 429
- McKee, C. 1993, in Back to the Galaxy, eds. S. Holt & F. Verter (New York: AIP Press), 499
- Meyer, D.M., Jura, M., Hawkins, I., & Cardelli, J.A. 1994, ApJ, 437, L59
- Milgrom, M. 1988, A&A, 202, L9
- Miralda-Escude, J., Cen, R., Ostriker, J.P. & Rauch, M. 1996, ApJ, 471, 582
- Miralda-Escude, J., & Rees, M. 1993, MNRAS, 260, 61
- Muller, C.A., Oort, J.H., & Raimond, E. 1963, C.R. Acad. Sci. Paris, 257, 1661
- Murakami, I., & Ikeuchi, S. 1990, PASJ, 41, L11
- Murphy, E.M., Lockman, F.J., & Savage, B.D. 1995, ApJ, 447, 642
- Mushotzky, R., Loewenstein, M., Arnaud, K., Tamura, T., Fukazawa, Y., Matsushita, K., Kikuchi, K., & Hatsukade, I. 1996, ApJ, 466, 686
- Oort, J.H. 1966, Bull. Astr. Inst. Netherlands, 18, 421
- Oort, J.H. 1970, A&A, 7, 381
- Oort, J.H. 1981, A&A, 94, 359
- Pilyugin, L.S., & Edmunds, M.G. 1996, A&A, 313, 792
- Rauch, M., Miralda-Escude, J., Sargent, W.L.W., Barlow, T.A., Weinberg, D.H., Hernquist, L., Katz, N., Cen, R., & Ostriker, J.P. 1997, ApJ, 489, 7
- Rauch, M., Weymann, R.J., & Morris, S.L. 1996, ApJ, 458, 518
- Raychaudhury, S., & Lynden-Bell, D. (RL) 1989, MNRAS, 240, 195.
- Rees, M.J. 1986, MNRAS, 218, 25P

- Rees, M.J. 1988, in QSO Absorption Lines, eds. J.C. Blades et al. (Cambridge: Cambridge Univ. Press), 107
- Renzini, A. 1997, ApJ, 488, 35
- Reynolds, R.J. 1996, BAAS, 188, 31.05
- Savage, B.D., Lu, L., Bahcall, J.N., Bergeron, J., & Boksenberg, A. 1993, ApJ, 413, 116
- Schlegel, D.J., Finkbeiner, D.P., & Davis, M. 1997, astro-ph/9710327
- Schulman, E., Bregman, J.N., Brinks, E., & Roberts, M.R. 1996, AJ, 112, 960
- Sembach, K.R. & Savage, B.D. 1996, ARA&A, 34, 279
- Sembach, K.R., Savage, B.D., Lu, L., & Murphy, E.M. 1995, ApJ 451, 616
- Shapiro, P.R., & Field, G.B. 1976, ApJ, 205, 762
- Songaila, A., Bryant, W., & Cowie, L.L. 1989, ApJ, 345, L71
- Stark, A.A., Gammie, C.F., Wilson, R.W., Bally, J., Linke, R.A., Heiles, C., & Hurwitz, M. (BTL) 1992, ApJS, 79, 77
- Stoche, J.T., Shull, J.M., Penton, S., Donahue, M. & Carilli, C. 1995, ApJ, 451, 24
- Taylor, C.L., Brinks, E., Grashuis, R.M., & Skillman, E.D. 1995, ApJS, 99, 427
- Tufte, S.L., Reynolds, R.J., & Haffner, L.M. 1998, ApJ, in press
- Tufte, S.L., Reynolds, R.J., Haffner, L.M., Jaehning, K.P. 1996, BAAS, 188, 43.08
- Tytler, D., Fan, X.-M., & Burles, S. 1996, Nature, 381, 207
- van der Hulst, J.M., & Sancisi, R. 1988, AJ, 95, 1354
- van Gorkom, J.H., Carilli, C.L., Stoche, J.T., Perlman, E.S., & Shull, J.M. 1996, AJ, 112, 1397
- van Woerden, H., Wakker, B.P., Schwarz, U.J., Peletier, R., & Kalberla, P.M.W. 1998, in The Local Super Bubble, eds. D. Breitschwerdt & M. Freiberg (Berlin: Springer-Verlag), in press
- Verschuur, G.L. 1969, ApJ, 156, 771
- Verschuur, G.L., & Cram, X.X. 1973, ???
- Verschuur, G.L. 1975, ARA&A, 13, 257
- Vogel, S.N., Weymann, R., Rauch, M., & Hamilton, T. 1995, ApJ, 44-1, 162
- Wakker, B.P. 1991, A&A, 250, 499
- Wakker, B.P., & Bregman, J.N. 1990, in Interstellar Neutral Hydrogen at High Velocities, Ph.D. Thesis of B.P. Wakker, University of Groningen

- Wakker, B.P., & Boulanger, F. 1986, *A&A*, 170, 84
- Wakker, B.P., Murphy, E.M., van Woerden, H., & Dame, T.M. 1997, *ApJ*, 488, 216
- Wakker, B.P., & Schwarz, U. 1991, *A&A*, 250, 484
- Wakker, B.P., & van Woerden, H. (WvW91) 1991, *A&A*, 250, 509
- Wakker, B.P., & van Woerden, H. (WvW97) 1997, *ARA&A*, 35, 217
- Wannier, P., & Wrixon, G.T. 1972, *ApJ*, 173, L119
- Wannier, P., Wrixon, G.T., & Wilson, R.W. 1972, *A&A*, 18, 224.
- Weaver, H. 1974, in *Highlights of Astronomy*, Vol. 3, ed. G. Contopoulos (Dordrecht: Reidel Pub. Co.), 423
- Weiner, B.J. 1998, private communication
- Weiner, B.J., & Williams, T.B. 1996, *AJ*, 111, 1156
- Wolfe, A.M. 1993, in *Relativistic Astrophysics and Cosmology*, eds. C.W. Akerlof & M.A. Srednicki (New York: NY Academy of Science), 281
- Wolfire, M.G., McKee, C.F., Hollenbach, D., & Tielens, A.G.G.M. 1995, *ApJ*, 453, 673
- Wright, M.C.H. 1974, *A&A*, 31, 317
- Wright, M.C.H. 1979, *ApJ*, 233, 35
- Zhang, Y., Anninos, P., & Norman, M.L. 1995, *ApJ*, 453, L57

This figure "fountain.gif" is available in "gif" format from:

<http://arxiv.org/ps/astro-ph/9803251v1>